

Generalized Three-Family Supersymmetric Pati-Salam Models from Type IIA Intersecting D6-Branes

Tianjun Li^{a,1} Qi Sun^{b,c,2} Rui Sun^{d,3} Lina Wu^{e,4}

^a*School of Physics, Henan Normal University, Xinxiang 453007, P. R. China*

^b*CAS Key Laboratory of Theoretical Physics, Institute of Theoretical Physics, Chinese Academy of Sciences, Beijing 100190, P. R. China*

^c*School of Physical Sciences, University of Chinese Academy of Sciences, No.19A Yuquan Road, Beijing 100049, P. R. China*

^d*School of Mathematical Sciences, University of Chinese Academy of Sciences, No.19A Yuquan Road, Beijing 100049, P. R. China*

^e*School of Sciences, Xi'an Technological University, Xi'an 710021, P. R. China*

E-mail: tli@itp.ac.cn, sunqi@itp.ac.cn, sunrui24@ucas.ac.cn, wulina@xatu.edu.cn

ABSTRACT:

Generalizing three-family chiral fermion conditions to $I_{ac} = -(3+h)$ and $I_{ac'} = h$, with positive integer h , we extend the landscape of three-family $\mathcal{N} = 1$ supersymmetric Pati-Salam models in a broader region. Differing from the former investigation with $I_{ac} = -3$ and $I_{ac'} = 0$, we do not restrict that the a stack of D6-branes must be parallel to the orientifold image of the c -stack along one of the three two-tori. In this investigation, without the simple parallel construction, we find four new classes of supersymmetric Pati-Salam models that are allowed by the extended three generation condition with $I_{ac} = 3, I_{ac'} = -6$ and $I_{ac} = -1, I_{ac'} = -2$ through the intersections of a - and c/c' -branes. Moreover, with the $SU(2)'_L$ gauge coupling realized from $SU(2)_{L_1} \times SU(2)_{L_2}$ symmetry breaking, the canonical normalization requirement of the gauge kinetic term provides an alternative approach that can be imposed before the renormalization group equation evolution for $SU(2)'_L$ gauge coupling. This turns out to be an effective mechanism to realize the string-scale gauge coupling relation, especially for the new supersymmetric Pati-Salam models with large g_b/g_a ratio. We show that this symmetry-breaking modified renormalization group evolution can highly suppress g_b/g_a , and finally realizes string-scale gauge coupling relations for the extended supersymmetric Pati-Salam models as well.

Contents

1	Introduction	1
2	Intersecting D6-branes Construction on $\mathbb{T}^6/(\mathbb{Z}_2 \times \mathbb{Z}_2)$ Orientifolds	3
3	Generalization of three-family Supersymmetric Pati-Salam Models	7
3.1	Intersecting Branes Model Building	10
3.2	Spectrum of Generalized Pati-Salam models	12
3.3	Gauge Coupling Relation Modified by Symmetry Breaking	15
4	Gauge Unification of Pati-Salam Generalization	16
4.1	String-scale Gauge Coupling Relations	18
4.2	Gauge Coupling Relation under Symmetry Breaking	19
5	Conclusions and Outlook	23
A	Generalized Supersymmetric Pati-Salam Models	29

1 Introduction

As one of the most important topics in string phenomenology, brane intersection theory has been investigated with great efforts from both string model building and phenomenology aspects [1–8]. From type IIA string theory, $\mathcal{N} = 1$ supersymmetric Pati-Salam models were constructed with orientifolds $\mathbb{T}^6/(\mathbb{Z}_2 \times \mathbb{Z}_2)$ from intersecting D6-branes as in [9–13]. In this construction, the gauge symmetries of $\mathcal{N} = 1$ supersymmetric Pati-Salam models, $SU(4)_C \times SU(2)_L \times SU(2)_R$, are realized from three stacks of D6-brane intersection, *i.e.*, a -, b -, and c -stacks which correspond to $SU(4)_C$, $SU(2)_L$, and $SU(2)_R$ gauge groups, respectively. The gauge symmetry can then be broken down to $SU(3)_C \times SU(2)_L \times U(1)_{B-L} \times U(1)_{I_{3R}}$ via D6-brane splitting. Without introducing any additional anomaly-free $U(1)$ around the electroweak scale, this gauge symmetry can be further broken down to Standard Model (SM) gauge symmetry via Higgs mechanism. And Yukawa couplings can be generated as well [14–27]. In Orbifold and Gepner configurations, D-brane vacua were also studied to realize SM [28]. From the phenomenology aspects, a cornerstone prediction of Grand Unified Theories (GUTs), is naturally realized in the Minimal Supersymmetric Standard Model (MSSM) [29–31], with the unification scale $M_{\text{GUT}} \sim 2 \times 10^{16}$ GeV. This scale differs from the typical string scale in weakly coupled heterotic string theory, which is an order of magnitude larger. As derived in [32], the string scale is given by

$$M_{\text{string}} = g_{\text{string}} \times 5.27 \times 10^{17} \text{ GeV}, \quad (1.1)$$

where string coupling constant $g_{string} \sim \mathcal{O}(1)$, implying $M_{string} \simeq 5 \times 10^{17}$ GeV. This introduces a factor of ~ 25 between M_U and M_{string} , posing a critical challenge in string phenomenology: how to obtain string-scale gauge coupling unification.

Since $\mathcal{N} = 1$ supersymmetric Pati-Salam models were constructed from intersecting D6-branes in Type IIA string theory, searching for the complete list of corresponding phenomenology models has been a long term topic for string phenomenology. From string theory perspective, this is related to the important string landscape problem investigated from various perspectives [33–42]. This has been investigated with random scanning methods, machine learning [43–52], and finally via systematic methods by means of solving diophantine equations for the wrapping numbers, the landscape of the standard Pati-Salam models were completed with 202752 number of $\mathcal{N} = 1$ supersymmetric Pati-Salam models found [53]. The string-scale coupling relations can also be realized in [54, 55] in the following work via two-loop Renormalization Group Equations (RGEs) evolution [56–60]. In which, there are in total 33 types of gauge coupling relations presented among the 202752 number of $\mathcal{N} = 1$ supersymmetric Pati-Salam models. In each class, these models are symmetrically related via type I/II T-dualities, D6-brane Sign Equivalent Principle (DSEP), and in particular there are four types of equivalent three generation relations due to symmetry transformation, such as $b \leftrightarrow b'$ and $c \leftrightarrow c'$. Therefore, models with quantum numbers $(\mathbf{4}, \mathbf{2}, \mathbf{1})$ and $(\bar{\mathbf{4}}, \mathbf{1}, \mathbf{2})$ under the gauge symmetries $SU(4)_C \times SU(2)_L \times SU(2)_R$ are considered with three generation conditions constrained by

$$\begin{aligned} I_{ab} + I_{ab'} &= 3, \\ I_{ac} &= -3, \quad I_{ac'} = 0, \end{aligned} \tag{1.2}$$

and

$$I_{ac} = 0, \quad I_{ac'} = -3. \tag{1.3}$$

Note that while $I_{ac'} = 0$, the stack a D6-branes must be parallel to the orientifold image of the c -stack along one of three two-tori. Similar parallel construction appears for the case of $I_{ac} = 0$ as well.

However, although the former landscape search of the standard Pati-Salam models are completed with all the string theory symmetries considered, the above three generation conditions may be further generalized. As proposed in [10], in addition to the completed search, potentially interesting constructions for Pati-Salam models, such as

$$I_{ac} = -(3 + h), \quad I_{ac'} = h, \tag{1.4}$$

with positive integer h , could also lead to the SM construction of three-family of chiral fermions. Namely, the former three generation conditions (1.2) and (1.3) may be simply generalized to

$$I_{ac} + I_{ac'} = -3, \tag{1.5}$$

with positive integer h , as the generalized three generation conditions. In this construction,

the massless vector-like Higgs fields are allowed, and the Pati-Salam gauge symmetry can be broken down to the SM gauge symmetry via the D6-brane splitting and Higgs mechanism. But it was also pointed in the former investigation that as large wrapping numbers are required to increase the value of I_{ac} and/or $I_{ac'}$, these type of models shall be rare. We refer to [10] for more detailed computing reason to the conclusion. That is why in the former investigations these models are not searched broadly in general. Be aware of this omission, here in this paper, we in particular search for the omitted models that allowed by the generalized three generation conditions (1.5).

In this new investigation, we also note that there is an isomorphism between the $SU(2)$ and $USp(2)$ groups. Such that, the Pati-Salam symmetry $SU(4) \times SU(2)_L \times SU(2)_R$ can be obtained from symmetry breaking of $SU(4) \times SU(2)_L \times SU(2)_R \times USp(2)$. In which, a diagonal $SU(2)'_L$ gauge group can be realized from the symmetry breaking of $SU(2)_L \times USp(2)$. As a rewarding outcome from this, the ratio of g_a and g_b denoted by $k_2 = g_b^2/g_a^2$ can be highly suppressed which helps to realize string-scale gauge coupling unification at M_{string} from the symmetry-breaking modified renormalization group evolution. In the manner of generic gauge coupling relations, the gauge coupling of the generalized supersymmetric Pati-Salam models can be represented by

$$g_a^2 = k_2 g_b^2 = k_Y g_Y^2 = g_U^2 \sim g_{\text{string}}^2, \quad (1.6)$$

where k_Y and k_2 are model-dependent constants that determine the weak mixing angle $\sin \theta_W$ at the string scale.

The paper is organized as follows. In Section 2, we briefly review the basic rules for supersymmetric model building from intersecting D6-branes on Type IIA orientifolds, with the tadpole cancellation conditions and $N = 1$ supersymmetry condition presented. In section 3, we introduce the generalization three-family conditions and the extended landscape of the supersymmetric Pati-Salam models. The $SU(2)_L \times USp(2)$ symmetry breaking which helps to suppress the gauge coupling is proposed in the end of this section as well. In section 4, we study in detail of the string-scale gauge coupling relation for the new Pati-Salam models with Renormalization Group Equations (RGEs) evolution. Finally, Section 5 is devoted to the conclusion and outlook, with the T-dual of the new Pati-Salam models presented in the Appendix.

2 Intersecting D6-branes Construction on $\mathbb{T}^6/(\mathbb{Z}_2 \times \mathbb{Z}_2)$ Orientifolds

D6-branes intersecting at generic angles on Type IIA $\mathbb{T}^6/(\mathbb{Z}_2 \times \mathbb{Z}_2)$ orientifolds have been investigated intensively to construct supersymmetric Pati-Salam models, such as in [36, 48]. Here the six-torus \mathbb{T}^6 can be decomposed into three two-tori $\mathbb{T}^6 = \mathbb{T}^2 \times \mathbb{T}^2 \times \mathbb{T}^2$, and thus the complex coordinates in the two-dimensional torus can be denoted as z_i , $i = 1, 2, 3$, respectively. The generators of the orbifold group $\mathbb{Z}_2 \times \mathbb{Z}_2$, θ and ω , correspond to the two vectors $(1/2, -1/2, 0)$ and $(0, 1/2, -1/2)$, respectively. They act on the complex coordinates

z_i , such that

$$\begin{aligned}\theta &: (z_1, z_2, z_3) \mapsto (-z_1, -z_2, z_3) , \\ \omega &: (z_1, z_2, z_3) \mapsto (z_1, -z_2, -z_3) .\end{aligned}\tag{2.1}$$

The orientifold projection is defined by gauging the ΩR symmetry, where Ω denotes the world-sheet parity and R represents the map with

$$R : (z_1, z_2, z_3) \mapsto (\bar{z}_1, \bar{z}_2, \bar{z}_3) .\tag{2.2}$$

The projection actions ΩR , $\Omega R\theta$, $\Omega R\omega$, and $\Omega R\theta\omega$ lead to different kinds of orientifold 6-planes (O6-planes). Moreover, N_a stacks of D6-branes wrapping on the factorized three-cycles can be introduced to cancel the RR charges of the O6-planes. And there are two possible complex structures that are consistent with orientifold projection on each two-torus: rectangular or tilted [34, 36, 48, 61]. The homology classes are represented by $n_a^i[a_i] + m_a^i[b_i]$ and $n_a^i[a'_i] + m_a^i[b_i]$ which correspond to rectangular and tilted tori, respectively, with $[a'_i] = [a_i] + \frac{1}{2}[b_i]$. Thus, in both cases, two wrapping numbers (n_a^i, l_a^i) are used to label a generic one cycle, where $l_a^i \equiv m_a^i$ for a rectangular two-torus and $l_a^i \equiv 2\tilde{m}_a^i = 2m_a^i + n_a^i$ on a tilted two-torus. Therefore, for tilted two-tours it is necessary that $l_a^i - n_a^i$ must be even.

In addition, for a - stack of N_a D6-branes along the cycle (n_a^i, l_a^i) , their ΩR images as a' - stack of N_a D6-branes are then labeled with wrapping numbers $(n_a^i, -l_a^i)$. And their homology three-cycles are represented by

$$[\Pi_a] = \prod_{i=1}^3 \left(n_a^i[a_i] + 2^{-\beta_i} l_a^i[b_i] \right) \quad \text{and} \quad [\Pi_{a'}] = \prod_{i=1}^3 \left(n_a^i[a_i] - 2^{-\beta_i} l_a^i[b_i] \right) ,\tag{2.3}$$

where $\beta_i = 0$ when the i -th torus is rectangular and $\beta_i = 1$ for tilted torus. The homology three-cycles wrapping on the four kinds of O6-planes can be represented by

$$\Omega R : [\Pi_{\Omega R}] = 2^3[a_1] \times [a_2] \times [a_3] ,\tag{2.4}$$

$$\Omega R\omega : [\Pi_{\Omega R\omega}] = -2^{3-\beta_2-\beta_3}[a_1] \times [b_2] \times [b_3] ,\tag{2.5}$$

$$\Omega R\theta\omega : [\Pi_{\Omega R\theta\omega}] = -2^{3-\beta_1-\beta_3}[b_1] \times [a_2] \times [b_3] ,\tag{2.6}$$

$$\Omega R\theta : [\Pi_{\Omega R}] = -2^{3-\beta_1-\beta_2}[b_1] \times [b_2] \times [a_3] .\tag{2.7}$$

Consequently, the intersection numbers between different stacks of D6-branes can be represented in terms of wrapping numbers such that

$$I_{ab} = [\Pi_a][\Pi_b] = 2^{-k} \prod_{i=1}^3 (n_a^i l_b^i - n_b^i l_a^i) ,\tag{2.8}$$

$$I_{ab'} = [\Pi_a][\Pi_{b'}] = -2^{-k} \prod_{i=1}^3 (n_a^i l_b^i + n_b^i l_a^i) ,\tag{2.9}$$

$$I_{aa'} = [\Pi_a] [\Pi_{a'}] = -2^{3-k} \prod_{i=1}^3 (n_a^i l_a^i), \quad (2.10)$$

$$I_{aO6} = [\Pi_a][\Pi_{O6}] = 2^{3-k} (-l_a^1 l_a^2 l_a^3 + l_a^1 n_a^2 n_a^3 + n_a^1 l_a^2 n_a^3 + n_a^1 n_a^2 l_a^3), \quad (2.11)$$

where $k = \beta_1 + \beta_2 + \beta_3$ denotes the total number of tilted two-tori while $\beta_i = 1$ for tilted tori and $\beta_i = 0$ for rectangular tori. And $[\Pi_{O6}] = [\Pi_{\Omega R}] + [\Pi_{\Omega R\omega}] + [\Pi_{\Omega R\theta\omega}] + [\Pi_{\Omega R\theta}]$ represents the sum of homology three-cycles associated with four O6-planes.

The generic massless particle spectrum on the intersecting D6-branes at general angles can be represented by the intersection numbers as summarized in Table 1, which holds for both rectangular and tilted two-tori configurations. The second column in the table specifies the representations under the gauge group $U(N_a/2)$ surviving under the $\mathbb{Z}_2 \times \mathbb{Z}_2$ orbifold projection [48]. All chiral supermultiplets contain both scalar and fermionic components in the supersymmetric configurations, and positive intersection numbers are adopted to denote the left-handed chiral supermultiplets.

Sector	Representation
aa	$U(N_a/2)$ vector multiplet 3 adjoint chiral multiplets
$ab + ba$	I_{ab} ($\square_a, \bar{\square}_b$) fermions
$ab' + b'a$	$I_{ab'}$ (\square_a, \square_b) fermions
$aa' + a'a$	$\frac{1}{2}(I_{aa'} - \frac{1}{2}I_{a,O6})$ $\square\square$ fermions $\frac{1}{2}(I_{aa'} + \frac{1}{2}I_{a,O6})$ \square fermions

Table 1. The general massless particle spectrum arising from D6-branes intersecting at generic angles is presented.

The four-dimensional $\mathcal{N} = 1$ Supersymmetric Conditions

In four-dimensional $\mathcal{N} = 1$ supersymmetric models, 1/4 supercharges from ten-dimensional Type I T-dual are restricted to be preserved. This preservation is required under the orientation projection of the intersecting D6-branes and the $\mathbb{Z}_2 \times \mathbb{Z}_2$ orbifold projection on the background manifold. Here any D6-brane rotation angle with respect to the orientifold plane shall be an element of $SU(3)$ for four-dimensional $\mathcal{N} = 1$ supersymmetry to survive under the orientation projection as in [2]. This is equivalent to $\theta_1 + \theta_2 + \theta_3 = 0 \pmod{2\pi}$, where θ_i is the angle between the D6-brane and the orientifold-plane in the i -th two-torus.

Moreover, we denote the products of wrapping numbers in a compact way to simplify the following discussion, such as

$$\begin{aligned} A_a &\equiv -n_a^1 n_a^2 n_a^3, & B_a &\equiv n_a^1 l_a^2 l_a^3, & C_a &\equiv l_a^1 n_a^2 l_a^3, & D_a &\equiv l_a^1 l_a^2 n_a^3, \\ \tilde{A}_a &\equiv -l_a^1 l_a^2 l_a^3, & \tilde{B}_a &\equiv l_a^1 n_a^2 n_a^3, & \tilde{C}_a &\equiv n_a^1 l_a^2 n_a^3, & \tilde{D}_a &\equiv n_a^1 n_a^2 l_a^3. \end{aligned} \quad (2.12)$$

Due to the $\mathbb{Z}_2 \times \mathbb{Z}_2$ orbifold projection automatically survive under such D6-brane config-

uration, the four-dimensional $\mathcal{N} = 1$ supersymmetry conditions read as in [36]

$$x_A \tilde{A}_a + x_B \tilde{B}_a + x_C \tilde{C}_a + x_D \tilde{D}_a = 0,$$

$$A_a/x_A + B_a/x_B + C_a/x_C + D_a/x_D < 0, \quad (2.13)$$

where $x_A = \lambda$, $x_B = \lambda 2^{\beta_2 + \beta_3} / \chi_2 \chi_3$, $x_C = \lambda 2^{\beta_1 + \beta_3} / \chi_1 \chi_3$, $x_D = \lambda 2^{\beta_1 + \beta_2} / \chi_1 \chi_2$, and the complex structure moduli with the i -th two-torus can be written in terms of $\chi_i = R_i^2 / R_i^1$. And a positive parameter λ can be introduced to put all variables A, B, C, D in an equivalent position.

The RR Tadpole Cancellation Conditions

As one of the most important condition for intersecting D-brane construction, the tadpole cancellation conditions directly lead to the $SU(N_a)^3$ cubic non-Abelian anomaly cancellation. And as discussed in [5, 6, 48], the Green-Schwarz mechanism mediated by untwisted RR fields can be used to cancel the U(1) mixed gauge and gravitational anomalies or $[SU(N_a)]^2$ U(1) gauge anomalies.

The RR fields arise from D6-branes and orientifold O6-planes which are restricted by the Gauss law in a compact space. The RR charges of D6-branes and D6-planes shall be canceled for conservation of the RR field flux lines, and thus the RR tadpole cancellation conditions can be represented by

$$\sum_a N_a [\Pi_a] + \sum_a N_a [\Pi_{a'}] - 4[\Pi_{O6}] = 0, \quad (2.14)$$

where the last terms are due to the O6-planes with -4 RR charges in the D6-brane charge unit. To cancel the RR tadpoles, an arbitrary number of D6-branes called "filler branes" wrapping along the orientifold planes can be introduced. And the RR tadpole cancellation conditions can be rewritten as

$$\begin{aligned} -2^k N^{(1)} + \sum_a N_a A_a &= -2^k N^{(2)} + \sum_a N_a B_a = \\ -2^k N^{(3)} + \sum_a N_a C_a &= -2^k N^{(4)} + \sum_a N_a D_a = -16, \end{aligned} \quad (2.15)$$

where $2N^{(i)}$ corresponds to the number of filler branes wrapping the i -th O6-plane. In addition, the filler branes realize the USp gauge group and share identical wrapping numbers with one of the four O6-planes as shown in Table 2. They also trivially contributes to the four-dimensional $\mathcal{N} = 1$ supersymmetry conditions.

Based on the above conditions, all possible D6-brane configurations can be classified into three categories under four-dimensional $\mathcal{N} = 1$ supersymmetry condition. The USp groups can be divided into A -, B -, C - or D -types based on whether their associated filler branes carry non-zero A, B, C or D , respectively.

- (1) In the case that the filler brane has the same wrapping numbers as one of the

Orientifold Action	O6-Plane	$(n^1, l^1) \times (n^2, l^2) \times (n^3, l^3)$
ΩR	1	$(2^{\beta_1}, 0) \times (2^{\beta_2}, 0) \times (2^{\beta_3}, 0)$
$\Omega R\omega$	2	$(2^{\beta_1}, 0) \times (0, -2^{\beta_2}) \times (0, 2^{\beta_3})$
$\Omega R\theta\omega$	3	$(0, -2^{\beta_1}) \times (2^{\beta_2}, 0) \times (0, 2^{\beta_3})$
$\Omega R\theta$	4	$(0, -2^{\beta_1}) \times (0, 2^{\beta_2}) \times (2^{\beta_3}, 0)$

Table 2. The wrapping numbers for four O6-planes.

O6-planes, the gauge symmetry is USp group and only one wrapping number product A , B , C and D has non-zero and negative value. We denote the corresponding USp group as the A -, B -, C - or D -type USp group according to which one is non-zero.

(2) In the case that there is a zero wrapping number, it is a Z-type D6-brane. A , B , C and D have two positive and two negative.

(3) In the case that there is no zero wrapping number, it is a NZ-type D6-brane. A , B , C and D have one positive and three negative. We denote NZ-type branes in the A -, B -, C - and D -type NZ branes by the positive one. Each type can be further divided into two subtypes by the wrapping numbers taking the form as follows

$$A1 : (-, -) \times (+, +) \times (+, +), \quad A2 : (-, +) \times (-, +) \times (-, +); \quad (2.16)$$

$$B1 : (+, -) \times (+, +) \times (+, +), \quad B2 : (+, +) \times (-, +) \times (-, +); \quad (2.17)$$

$$C1 : (+, +) \times (+, -) \times (+, +), \quad C2 : (-, +) \times (+, +) \times (-, +); \quad (2.18)$$

$$D1 : (+, +) \times (+, +) \times (+, -), \quad D2 : (-, +) \times (-, +) \times (+, +). \quad (2.19)$$

For convenience, we call Z-type and NZ-type D6-branes as U -branes because they have gauge symmetry $U(n)$.

3 Generalization of three-family Supersymmetric Pati-Salam Models

Two extra $U(1)$ gauge groups are needed when one obtains SM or standard-like models by intersecting D6-branes. As a result, right-handed charged leptons obtain the correct quantum number in both supersymmetric and non-supersymmetric models [6, 35, 36, 48]. These two groups are, respectively, the lepton number symmetry $U(1)_L$ and the third component of the right-handed weak isospin $U(1)_{I_{3R}}$. And the hypercharge Q_Y is related to the the baryonic charge Q_B as

$$Q_Y = Q_{I_{3R}} + \frac{Q_B - Q_L}{2}, \quad (3.1)$$

where Q_B is generated by the decomposition $U(3)_C \simeq SU(3)_C \times U(1)_B$. The gauge group $U(1)_{I_{3R}}$ comes from the non-abelian component of the symmetry $U(2)_R$ or USp due to the massless gauge field of $U(1)_{I_{3R}}$. Otherwise, $U(1)_{I_{3R}}$ will get mass from the $B \wedge F$ couplings. Similarly, an anomaly-free $U(1)_{B-L}$ must come from the non-abelian group,

and in previous related work on supersymmetric model building, $U(1)_{I_{3R}}$ comes from the USp groups [35, 48].

These models actually possess two anomaly-free $U(1)$ symmetries and are configured with no less than eight Higgs doublets. Although it is theoretically possible to achieve the breaking of its symmetry group to SM, this process will inevitably lead to violating of the D-flatness and F-flatness, thereby inevitably losing supersymmetry. We consider a configuration of three distinct D6-brane stacks denoted by a, b, and c, comprising 8, 4, and 4 D6-branes, respectively. The associated gauge symmetries are $U(4)_C \times U(2)_L$ and $U(2)_R$, giving rise to the Pati–Salam gauge group $SU(4)_C \times SU(2)_L \times SU(2)_R$. As outlined in [10], through a combination of D6-brane splitting and the Higgs mechanism, this symmetry can be broken down to the SM gauge group according to the following symmetry-breaking chain:

$$\begin{aligned} SU(4) \times SU(2)_L \times SU(2)_R &\xrightarrow{a \rightarrow a_1 + a_2} SU(3)_C \times SU(2)_L \times SU(2)_R \times U(1)_{B-L} \\ &\xrightarrow{c \rightarrow c_1 + c_2} SU(3)_C \times SU(2)_L \times U(1)_{I_{3R}} \times U(1)_{B-L} \\ &\xrightarrow{\text{Higgs Mechanism}} SU(3)_C \times SU(2)_L \times U(1)_Y. \end{aligned} \quad (3.2)$$

The phenomenon of dynamical supersymmetry breaking has been investigated in [39] within the framework of D6-brane constructions derived from Type IIA orientifolds. For a D6-brane stack labeled a, the corresponding kinetic function takes the following form [34]:

$$f_a = \frac{1}{4\kappa_a} \left(n_a^1 n_a^2 n_a^3 s - \frac{n_a^1 l_a^2 l_a^3 u^1}{2^{\beta_2 + \beta_3}} - \frac{l_a^1 n_a^2 l_a^3 u^2}{2^{\beta_1 + \beta_3}} - \frac{l_a^1 l_a^2 n_a^3 u^3}{2^{\beta_1 + \beta_2}} \right), \quad (3.3)$$

where κ_a is a constant with respect to the gauge groups, as an example $\kappa_a = 1$ for $SU(N_a)$. We work with the moduli parameter s and u^i (with $i = 1, 2, 3$) in the supergravity basis, which are connected to the four-dimensional dilaton ϕ_4 and the moduli parameters of complex structure U_i (with $i = 1, 2, 3$) through the following relations:

$$\begin{aligned} \text{Re}(s) &= \frac{e^{-\phi_4}}{2\pi} \frac{\sqrt{\text{Im}(U^1) \text{Im}(U^2) \text{Im}(U^3)}}{|U^1 U^2 U^3|}, \\ \text{Re}(u^1) &= \frac{e^{-\phi_4}}{2\pi} \sqrt{\frac{\text{Im}(U^1)}{\text{Im}(U^2) \text{Im}(U^3)}} \left| \frac{U^2 U^3}{U^1} \right|, \\ \text{Re}(u^2) &= \frac{e^{-\phi_4}}{2\pi} \sqrt{\frac{\text{Im}(U^2)}{\text{Im}(U^1) \text{Im}(U^3)}} \left| \frac{U^1 U^3}{U^2} \right|, \\ \text{Re}(u^3) &= \frac{e^{-\phi_4}}{2\pi} \sqrt{\frac{\text{Im}(U^3)}{\text{Im}(U^1) \text{Im}(U^2)}} \left| \frac{U^1 U^2}{U^3} \right|. \end{aligned} \quad (3.4)$$

In the current model, the complex structures U^i (with $i = 1, 2, 3$) can be written in term

of the moduli parameters as [34]

$$U^1 = i\chi_1, \quad U^2 = i\chi_2, \quad U^3 = \frac{2\chi_3^2 + 4i\chi_3}{4 + \chi_3^2}, \quad (3.5)$$

where χ_1, χ_2 , and χ_3 are not independent degrees of freedom, as they can be fully expressed through the parameters x_A, x_B, x_C, x_D which themselves are constrained by the supersymmetric condition given in (2.13). In practice, these χ_i parameters are determined only up to an overall coefficient, reflecting freedom under a dilation transformation. The Kähler potential is given by

$$K = -\ln(S + \bar{S}) - \sum_{i=1}^3 \ln(U^i + \bar{U}^i). \quad (3.6)$$

The complete determination of all moduli parameters, therefore, requires the stabilization of this dilation degree of freedom.

In this approach, gaugino condensation is often utilized to fix the overall coefficient, and at least two USp groups are usually presented in the hidden sector such as discussed in [62–64]. And the one-loop beta functions are described in [10] as

$$\beta_i^g = -3 \left(\frac{N^{(i)}}{2} + 1 \right) + 2|I_{ai}| + |I_{bi}| + |I_{ci}| + 3 \left(\frac{N^{(i)}}{2} - 1 \right) = -6 + 2|I_{ai}| + |I_{bi}| + |I_{ci}|. \quad (3.7)$$

For each USp($N^{(i)}$) group originated from $2N^{(i)}$ filler branes, the corresponding one-loop beta functions must be negative. In the present work, we do not confine our analysis to configurations containing at least two USp groups in the hidden sectors, to accommodate other prospective symmetry-breaking mechanisms. The gauge coupling constant associated with stack a of the D6-branes can be given by

$$g_a^{-2} = |\text{Re}(f_a)|, \quad (3.8)$$

and as follows the gauge couplings for stacks b and c of the D6-branes are obtained in the same way. The kinetic function associated with the $U(1)_Y$ gauge group is a linear combination of the kinetic functions corresponding to the $SU(4)_C$ and $SU(2)_R$ groups, as established in [34, 61]

$$f_Y = \frac{3}{5} \left(\frac{2}{3} f_a + f_c \right), \quad (3.9)$$

while the coupling constant g_Y is determined by

$$g_Y^{-2} = |\text{Re}(f_Y)|. \quad (3.10)$$

At the tree level, the gauge coupling relation reads

$$g_a^2 = \alpha g_b^2 = \beta \frac{5}{3} g_Y^2 = \gamma (\pi e^{\phi_4}), \quad (3.11)$$

where α , β , and γ denote the ratios between the strong, weak, and hypercharge couplings, respectively. And here the ϕ^4 represents the dilaton field.

3.1 Intersecting Branes Model Building

Recall that for brane intersecting construction, a systematic searching algorithm has been constructed in [53], with the standard Pati-Salam landscape completely given. In which, each Pati-Salam model is determined by 18 integer wrapping numbers $n_a^1, \dots, n_c^3, l_a^1, \dots, l_c^3$.

In our new Pati-Salam model building with the generalized three-family condition $I_{ab} + I_{ab'} = 3, I_{ac} + I_{ac'} = -3$, these wrapping numbers are still restricted by the condition of tadpole cancellation (2.15), supersymmetry condition (2.13). Still, the wrapping number relation $l_a^1 - n_a^1$ shall be even while the corresponding torus is tilted. Utilizing the first parts of the systematic searching method in [53], we revise for the generalized Pati-Salam model building as follows:

First step: we still list the sign of wrapping number products $A_a, B_a, \dots, C_c, C_d$. As discussed in [36, 53], due to the supersymmetry constraints, there are three type of possible signs for wrapping number products (A_a, B_a, C_a, D_a) of each $a/b/c$ - stacks of brane construction: three negative numbers and one positive number; two negative numbers and two zeroes; one negative number and three zeros.

Second step: for each possible sign in the first step, we divide the whole problem into categories according to the inequalities of wrapping number products, such as $A_a > 0, B_a < 0, C_a < 0, D_a < 0$, and try to solve the values of the wrapping numbers. In each category, we first solve the generalized three family relation such that:

1. Equation of the form $I_{ac} + I_{ac'} = -3$. This includes additional $I_{ac} = -1, I_{ac'} = -2$, or $I_{ac} = 3, I_{ac'} = -6, \dots$, (other than the usual $I_{ac} = -3, I_{ac'} = 0$), and vice versa for the value of I_{ac} , and $I_{ac'}$. From the definition of I_{ab} and $I_{ab'}$, we consider $\prod_{i=1}^3 (n_a^i l_c^i - l_a^i n_c^i)$, $\prod_{i=1}^3 (n_a^i l_c^i + l_a^i n_c^i)$ and naturally take $n_a^i l_c^i - l_a^i n_c^i$, $i = 1, 2, 3$ as variables.
2. Under the additional solutions of above, solve the equation of $I_{ab} + I_{ab'} = 3$. Again, consider $\prod_{i=1}^3 (n_a^i l_c^i - l_a^i n_c^i)$, $\prod_{i=1}^3 (n_a^i l_c^i + l_a^i n_c^i)$ and naturally take $n_a^i l_c^i - l_a^i n_c^i$, $i = 1, 2, 3$ as variables.
3. Different with the former system of linear equations of full rank, the new solution of model building does not include

$$\begin{cases} n_a^1 l_c^1 - l_a^1 n_c^1 = 0 \\ n_a^1 l_c^1 + l_a^1 n_c^1 = 6, \end{cases}$$

while

$$\begin{cases} n_a^1 l_b^1 - l_a^1 n_b^1 = 0 \\ n_a^1 l_b^1 + l_a^1 n_b^1 = 6, \end{cases}$$

are still presented in this extension with $n_a^1 l_b^1$ and $l_a^1 n_b^1$ as variables. From the former research, we know that this kind of equations has unique solutions.

4. For each type of the linear inequalities derived from the first step, we could still see a subsystem in the form of

$$\begin{cases} 4 + 2A_a + A_b + A_c \geq 0 \\ A_a < 0 \\ A_b < 0 \\ A_c = 0. \end{cases}$$

For each type of linear inequalities listed in Step 1, the integers solution system corresponds to a polyhedron, and whether the polyhedron has finite volume corresponds to whether we have a finite number of solutions/models.

According to the restrictions from these inequalities, the total number of unknown wrapping numbers decrease. Part of the systems are split into subsystems as here the inequalities can not uniquely determine the values of the 18 wrapping numbers.

Third step: By repeating the Second step for each type of inequalities we find 4 classes of new Pati-Salam models as show in Table 3, 4, 5, 6 from the three-family generalization as follows¹.

Table 3. D6-brane configurations and intersection numbers of Model 1, and its MSSM gauge coupling relation is $g_a^2 = \frac{7}{6}g_b^2 = \frac{35}{66}g_c^2 = \frac{175}{268}(\frac{5}{3}g_Y^2) = \frac{8\sqrt{25}^{3/4}\pi e^{\phi_4}}{11\sqrt{3}}$.

model 1	$U(4) \times U(2)_L \times U(2)_R \times USp(2)$								
stack	N	$(n^1, l^1) \times (n^2, l^2) \times (n^3, l^3)$	$n_{\square\square}$	n_{\square}	b	b'	c	c'	1
a	8	$(1, 1) \times (1, 0) \times (1, -1)$	0	0	3	0	3	-6	0
b	4	$(1, -1) \times (1, -1) \times (1, 2)$	-2	-6	-	-	8	0	2
c	4	$(-1, 5) \times (0, 1) \times (-1, 2)$	9	-9	-	-	-	-	10
1	2	$(2, 0) \times (1, 0) \times (1, 0)$	$x_A = \frac{1}{12}x_B = \frac{1}{10}x_C = \frac{1}{12}x_D$ $\beta_1^g = 6$ $\chi_1 = \frac{1}{\sqrt{10}}, \chi_2 = \frac{\sqrt{5}}{6}, \chi_3 = \sqrt{\frac{2}{5}}$						

Table 4. D6-brane configurations and intersection numbers of Model 2, and its MSSM gauge coupling relation is $g_a^2 = \frac{11}{6}g_b^2 = \frac{5}{14}g_c^2 = \frac{25}{52}(\frac{5}{3}g_Y^2) = \frac{8}{63}5^{3/4}\sqrt{11}\pi e^{\phi_4}$.

model 2	$U(4) \times U(2)_L \times U(2)_R \times USp(2)^2$									
stack	N	$(n^1, l^1) \times (n^2, l^2) \times (n^3, l^3)$	$n_{\square\square}$	n_{\square}	b	b'	c	c'	1	4
a	8	$(-1, 1) \times (-1, 1) \times (-1, 1)$	0	4	0	3	3	-6	1	1
b	4	$(-2, 1) \times (0, 1) \times (-1, 1)$	-1	1	-	-	9	-10	1	0
c	4	$(-1, 2) \times (-1, 0) \times (5, 1)$	9	-9	-	-	-	-	0	1
1	2	$(1, 0) \times (1, 0) \times (2, 0)$	$x_A = 22x_B = 2x_C = \frac{11}{5}x_D$ $\beta_1^g = -3, \beta_4^g = -3$ $\chi_1 = \frac{1}{\sqrt{5}}, \chi_2 = \frac{11}{\sqrt{5}}, \chi_3 = 4\sqrt{5}$							
4	2	$(0, 1) \times (0, 1) \times (2, 0)$								

¹Here we note that for each model, there is a class of physical equivalent generalized models according to the gauge coupling relations.

Table 5. D6-brane configurations and intersection numbers of Model 3, and its MSSM gauge coupling relation is $g_a^2 = 3g_b^2 = \frac{13}{5}g_c^2 = \frac{65}{41}(\frac{5}{3}g_Y^2) = \frac{16}{5}\sqrt{3}\pi e^{\phi_4}$.

model 3	$U(4) \times U(2)_L \times U(2)_R \times USp(2) \times USp(4)$									
stack	N	$(n^1, l^1) \times (n^2, l^2) \times (n^3, l^3)$	$n_{\square\square}$	n_{\square}	b	b'	c	c'	1	3
a	8	$(-1, 1) \times (-1, 0) \times (1, 1)$	0	0	3	0	-1	-2	0	0
b	4	$(-1, 4) \times (0, 1) \times (-1, 1)$	3	-3	-	-	-8	4	4	1
c	4	$(1, 0) \times (1, -1) \times (1, 3)$	-2	2	-	-	-	-	0	1
1	2	$(1, 0) \times (1, 0) \times (2, 0)$	$x_A = \frac{3}{4}x_B = \frac{1}{4}x_C = \frac{3}{4}x_D$ $\beta_1^g = -2, \beta_3^g = -4$ $\chi_1 = \frac{1}{2}, \chi_2 = \frac{3}{2}, \chi_3 = 1$							
3	4	$(0, 1) \times (1, 0) \times (0, 2)$								

Table 6. D6-brane configurations and intersection numbers of Model 4, and its MSSM gauge coupling relation is $g_a^2 = 6g_b^2 = \frac{26}{5}g_c^2 = \frac{130}{67}(\frac{5}{3}g_Y^2) = \frac{16}{5}\sqrt{6}\pi e^{\phi_4}$.

model 4	$U(4) \times U(2)_L \times U(2)_R \times USp(4)$									
stack	N	$(n^1, l^1) \times (n^2, l^2) \times (n^3, l^3)$	$n_{\square\square}$	n_{\square}	b	b'	c	c'	3	
a	8	$(-1, 1) \times (-1, 0) \times (1, 1)$	0	0	3	0	-1	-2	0	
b	4	$(-1, 4) \times (0, 1) \times (-1, 1)$	3	-3	-	-	-16	8	1	
c	4	$(1, 0) \times (2, -1) \times (1, 3)$	-5	5	-	-	-	-	1	
3	4	$(0, 1) \times (1, 0) \times (0, 2)$	$x_A = \frac{3}{2}x_B = \frac{1}{4}x_C = \frac{3}{2}x_D$ $\beta_3^g = -4$ $\chi_1 = \frac{1}{2}, \chi_2 = 3, \chi_3 = 1$							

3.2 Spectrum of Generalized Pati-Salam models

The gauge symmetry for these four classes of extended Pati-Salam models are still $U(4) \times U(2)_L \times U(2)_R$ as the standard construction, yet with only one, and two confining groups. Different with the former Pati-Salam models, three and four confining groups are not observed. While there are four confining gauge groups in the hidden sector with four negative β functions appearing, one can break supersymmetry via gaugino condensation. For models in Table 4 and 5, there are two negative β functions with two confining $USp(N)$ gauge groups, a general analysis of the non-perturbative superpotential with tree-level gauge couplings and moduli stabilization according to dilaton and complex structure moduli can be investigated, as discussed in [39]. However, we shall note that these extrema from moduli stabilization might be saddle points that does not lead to supersymmetry breaking, while at the stable extremum the supersymmetry can be broken in general.

Now we take the representative models of these 4 classes in tables 3 to 6 as examples to discuss the full spectrum explicitly. Their gauge coupling unification from RGEs will be left to discuss in the next section with $SU(3)_C \times SU(2)_L \times U(1)_Y$ gauge coupling unification at the near string scale.

From the spectrum of Model 1, the Higgs up and down doublets arise from the intersection of b -stack and the image of c -stack of branes. However, as the β function of $USp(2)$ group is positive, it is not confining which leads to difficulty for dynamical supersymmetry breaking in model building. Therefore, we do not focus on this class of models for further

Table 7. The chiral spectrum in the open string sector of Model 1

model 1	$SU(4) \times SU(2)_L \times SU(2)_R \times USp(2)$	Q_4	Q_{2L}	Q_{2R}	Q_{em}	$B - L$	Field
ab	$3 \times (4, \bar{2}, 1, 1)$	1	-1	0	$-\frac{1}{3}, \frac{2}{3}, -1, 0$	$\frac{1}{3}, -1$	Q_L, \bar{L}_L
ac	$3 \times (4, 1, \bar{2}, 1)$	1	0	-1	$-\frac{1}{3}, \frac{2}{3}, -1, 0$	$\frac{1}{3}, -1$	\bar{Q}_R, \bar{L}_R
ac'	$6 \times (\bar{4}, 1, \bar{2}, 1)$	-1	0	-1	$\frac{1}{3}, -\frac{2}{3}, 1, 0$	$-\frac{1}{3}, 1$	Q_R, L_R
bc	$8 \times (1, 2, \bar{2}, 1)$	0	1	-1	$1, 0, 0, -1$	0	H'
$b1$	$2 \times (1, 2, 1, \bar{2})$	0	1	0	$\pm \frac{1}{2}$	0	
$c1$	$10 \times (1, 1, 2, \bar{2})$	0	0	1	$\pm \frac{1}{2}$	0	
b 	$2 \times (1, \bar{3}, 1, 1)$	0	-2	0	$0, \pm 1$	0	
\bar{b} 	$6 \times (1, \bar{1}, 1, 1)$	0	-2	0	0	0	
c 	$9 \times (1, 1, 3, 1)$	0	0	2	$0, \pm 1$	0	
\bar{c} 	$9 \times (1, 1, \bar{1}, 1)$	0	0	-2	0	0	
bc'	$3 \times (1, 2, 2, 1)$	0	1	1	$1, 0, 0, -1$	0	H_u^i, H_d^i
	$3 \times (1, \bar{2}, \bar{2}, 1)$	0	-1	-1			

phenomenology study. For the spectrum of Model 2, the Higgs doublets can be not arise from the intersection of b -stack and c -stack of branes, either the intersection of b -stack and the image of c -stack of branes. However, the β function of its two $USp(2)$ groups are negative with possible confining groups leading to stable minimum for supersymmetry breaking.

Table 8. The chiral spectrum in the open string sector of Model 2

model 2	$SU(4) \times SU(2)_L \times SU(2)_R \times USp(2)^2$	Q_4	Q_{2L}	Q_{2R}	Q_{em}	$B - L$	Field
ab'	$3 \times (4, 2, 1, 1, 1)$	1	1	0	$-\frac{1}{3}, \frac{2}{3}, -1, 0$	$\frac{1}{3}, -1$	Q_L, \bar{L}_L
ac	$3 \times (4, 1, \bar{2}, 1, 1)$	1	0	-1	$-\frac{1}{3}, \frac{2}{3}, -1, 0$	$\frac{1}{3}, -1$	\bar{Q}_R, \bar{L}_R
ac'	$6 \times (\bar{4}, 1, \bar{2}, 1, 1)$	-1	0	-1	$\frac{1}{3}, -\frac{2}{3}, 1, 0$	$-\frac{1}{3}, 1$	Q_R, L_R
bc	$9 \times (1, 2, \bar{2}, 1, 1)$	0	1	-1	$1, 0, 0, -1$	0	H'
bc'	$10 \times (1, \bar{2}, \bar{2}, 1, 1)$	0	-1	-1	$1, 0, 0, -1$	0	H''
$a1$	$1 \times (4, 1, 1, \bar{2}, 1)$	1	0	0	$\frac{1}{6}, -\frac{1}{2}$	$\frac{1}{3}, -1$	
$a4$	$1 \times (4, 1, 1, 1, \bar{2})$	1	0	0	$\frac{1}{6}, -\frac{1}{2}$	$\frac{1}{3}, -1$	
$b1$	$1 \times (1, 2, 1, \bar{2}, 1)$	0	1	0	$\pm \frac{1}{2}$	0	
$c4$	$1 \times (1, 1, 2, 1, \bar{2})$	0	0	1	$\pm \frac{1}{2}$	0	
a 	$4 \times (6, 1, 1, 1, 1)$	2	0	0	$-\frac{1}{3}, 1$	$-\frac{2}{3}, 2$	
b 	$1 \times (1, \bar{3}, 1, 1, 1)$	0	-2	0	$0, \pm 1$	0	
\bar{b} 	$1 \times (1, 1, 1, 1, 1)$	0	2	0	0	0	
c 	$9 \times (1, 1, 3, 1, 1)$	0	0	2	$0, \pm 1$	0	
\bar{c} 	$9 \times (1, 1, \bar{1}, 1, 1)$	0	0	-2	0	0	

In the class of Model 3, the representative model has 8 Higgs multiplets naturally arising from the intersection of b -stack and c -stack of branes, also with relatively few exotic particles beyond SM. The β function of its $USp(2)$ and $USp(4)$ groups are negative with

Table 9. The chiral spectrum in the open string sector of Model 3

model 3	$SU(4) \times SU(2)_L \times SU(2)_R$ $\times USp(2) \times USp(4)$	Q_4	Q_{2L}	Q_{2R}	Q_{em}	$B - L$	Field
ab	$3 \times (4, \bar{2}, 1, 1, 1)$	1	-1	0	$-\frac{1}{3}, \frac{2}{3}, -1, 0$	$\frac{1}{3}, -1$	Q_L, L_L
ac	$1 \times (\bar{4}, 1, 2, 1, 1)$	-1	0	1	$\frac{1}{3}, -\frac{2}{3}, 1, 0$	$-\frac{1}{3}, 1$	Q_R, L_R
ac'	$2 \times (\bar{4}, 1, \bar{2}, 1, 1)$	-1	0	-1	$\frac{1}{3}, -\frac{2}{3}, 1, 0$	$-\frac{1}{3}, 1$	Q_R, L_R
bc	$8 \times (1, \bar{2}, 2, 1, 1)$	0	-1	1	1, 0, 0, -1	0	H'
bc'	$4 \times (1, 2, 2, 1, 1)$	0	1	1	1, 0, 0, -1	0	H
$b1$	$4 \times (1, 2, 1, \bar{2}, 1)$	0	1	0	$\pm \frac{1}{2}$	0	
$b3$	$1 \times (1, 2, 1, 1, \bar{4})$	0	1	0	$\pm \frac{1}{2}$	0	
$c3$	$1 \times (1, 1, 2, 1, \bar{4})$	0	0	1	$\pm \frac{1}{2}$	0	
$b \begin{array}{ c } \hline \square \\ \hline \end{array}$	$3 \times (1, 3, 1, 1, 1)$	0	2	0	0, ± 1	0	
$\bar{b} \begin{array}{ c } \hline \square \\ \hline \end{array}$	$3 \times (1, \bar{1}, 1, 1, 1)$	0	-2	0	0	0	
$c \begin{array}{ c } \hline \square \\ \hline \end{array}$	$2 \times (1, 1, \bar{3}, 1, 1)$	0	0	-2	0, ± 1	0	
$\bar{c} \begin{array}{ c } \hline \square \\ \hline \end{array}$	$2 \times (1, 1, 1, 1, 1)$	0	0	2	0	0	

possible confining groups leading to stable minimum for supersymmetry breaking as well.

Table 10. The composite particle spectrum of Model 3, which is formed due to the strong forces from hidden sector.

Model 3		$SU(4) \times SU(2)_L \times SU(2)_R \times USp(2) \times USp(4)$	
Confining Force	Intersection	Exotic Particle Spectrum	Confined Particle Spectrum
$USp(2)_1$	$b1$	$4 \times (1, 2, 1, 2, 1)$	$8 \times (1, 2^2, 1, 1, 1)$
$USp(2)_3$	$b3$	$1 \times (1, 2, 1, 1, 2)$	$1 \times (1, 2^2, 1, 1, 1), 1 \times (1, 2, 2, 1, 1)$
	$c3$	$1 \times (1, 1, 2, 1, 2)$	$1 \times (1, 1, 2^2, 1, 1)$

Model 3 has two confining gauge groups, $USp(2)_1$ and $USp(4)_3$. For $USp(2)_2$, there is only one charged intersection, and $USp(4)_3$ has two charged intersections. Therefore, for $USp(2)_1$, there is no mixed-confinement, their self-confinement leads to 8 tensor representations for each of them. While $USp(4)_3$ has two charged intersections, and therefore besides self-confinement, the mixed-confinement between different intersections also exist, which yields the chiral supermultiplets $(1, 2, 2, 1, 1)$. Moreover, these spectra of models are anomaly-free as there is no new anomaly introduced to the remaining gauge symmetry [37].

For the class of Model 4, the representative model in Table 6 has the spectrum in Table 11 with 8 Higgs multiplets naturally arising from the intersection of b -stack and the image of c -stack of branes. The β function of its single $USp(4)$ group is negative with possible confining groups leading to stable minimum for supersymmetry breaking as well. As $USp(4)_3$ has two charged intersections, and thus besides self-confinement leading to tensor representations, the mixed-confinement between different intersection exists and yields to the chiral supermultiplets $(1, 2, 2, 1)$.

Table 11. The chiral spectrum in the open string sector of Model 4

model 4	$SU(4) \times SU(2)_L \times SU(2)_R \times USp(4)$	Q_4	Q_{2L}	Q_{2R}	Q_{em}	$B - L$	Field
ab	$3 \times (4, \bar{2}, 1, 1)$	1	-1	0	$-\frac{1}{3}, \frac{2}{3}, -1, 0$	$\frac{1}{3}, -1$	Q_L, L_L
ac	$1 \times (\bar{4}, 1, 2, 1)$	-1	0	1	$-\frac{1}{3}, -\frac{2}{3}, 1, 0$	$-\frac{1}{3}, 1$	Q_R, L_R
ac'	$2 \times (\bar{4}, 1, \bar{2}, 1)$	-1	0	-1	$\frac{1}{3}, -\frac{2}{3}, 1, 0$	$-\frac{1}{3}, 1$	Q_R, L_R
bc	$16 \times (1, \bar{2}, 2, 1)$	0	-1	1	$1, 0, 0, -1$	0	H'
bc'	$8 \times (1, 2, 2, 1)$	0	1	1	$1, 0, 0, -1$	0	H
$b3$	$1 \times (1, 2, 1, \bar{4})$	0	1	0	$\pm \frac{1}{2}$	0	
$c3$	$1 \times (1, 1, 2, \bar{4})$	0	0	1	$\pm \frac{1}{2}$	0	
$b \begin{array}{ c } \hline \square \\ \hline \end{array}$	$3 \times (1, 3, 1, 1)$	0	2	0	$0, \pm 1$	0	
$\bar{b} \begin{array}{ c } \hline \square \\ \hline \end{array}$	$3 \times (1, \bar{1}, 1, 1)$	0	-2	0	0	0	
$c \begin{array}{ c } \hline \square \\ \hline \end{array}$	$5 \times (1, 1, \bar{3}, 1)$	0	0	-2	$0, \pm 1$	0	
$\bar{c} \begin{array}{ c } \hline \square \\ \hline \end{array}$	$5 \times (1, 1, 1, 1)$	0	0	2	0	0	

Table 12. The composite particle spectrum of Model 4, which is formed due to the strong forces from hidden sector.

Model 4		$SU(4) \times SU(2)_L \times SU(2)_R \times USp(4)$	
Confining Force	Intersection	Exotic Particle Spectrum	Confined Particle Spectrum
$USp(4)_3$	$b3$	$1 \times (1, 2, 1, 2)$	$1 \times (1, 2^2, 1, 1), 1 \times (1, 2, 2, 1)$
	$c3$	$1 \times (1, 1, 2, 2)$	$1 \times (1, 1, 2^2, 1)$

3.3 Gauge Coupling Relation Modified by Symmetry Breaking

The $SU(2)_{L_1} \times SU(2)_{L_2}$ symmetry can be broken down to the diagonal subgroup $SU(2)_{L'}$ through the mechanism of vacuum expectation values. Specifically, if the gauge couplings of the two subgroups $SU(2)_{L_1}$ and $SU(2)_{L_2}$ are g_{L_1} and g_{L_2} , respectively, the coupling constant $g_{L'}$ of the resulting diagonal subgroup $SU(2)$ after breaking satisfies

$$\frac{1}{g_{L'}} = \frac{1}{g_{L_1}} + \frac{1}{g_{L_2}}. \quad (3.12)$$

This relation stems from the canonical normalization requirement of the gauge kinetic terms after symmetry breaking. Within the framework of the holomorphic gauge kinetic function, the gauge kinetic function for the diagonal subgroup can be written as

$$f_{L'} = f_{L_1} + f_{L_2}. \quad (3.13)$$

In this way, to some extent, we can suppress the value of the $g_{L'}$ coupling for the overall $SU(2)_{L'}$. For instance, we can introduce the filler brane on type-1 O6-plane as the d-stack. Taking Model 2 as an example, due to the isomorphism between the $SU(2)$ and $USp(2)$ groups, we can obtain the Pati-Salam model symmetry $SU(4) \times SU(2)_L \times SU(2)_R$ from $SU(4) \times SU(2)_L \times SU(2)_R \times USp(2)_1$ by the mechanism of symmetry breaking from $SU(2)_L \times USp(2)_1$ to the diagonal $SU(2)_{L'}$. By comparing the gauge coupling relations of

Model 2 and the suppressed gauge coupling relations resulting from symmetry breaking as shown in Model 2-m in Table 13, one can see that the value of the $g_{L'}$ coupling, which is g_b in model 2, is significantly suppressed.

Table 13. D6-brane configurations and intersection numbers of Model 2-m, and its MSSM gauge coupling relation is $g_a^2 = \frac{55}{723}g_L^2 = \frac{5}{14}g_c^2 = \frac{25}{52}(\frac{5}{3}g_Y^2) = \frac{8}{63}5^{3/4}\sqrt{11}\pi e^{\phi_4}$.

model 2-m	$U(4) \times U(2)_L \times U(2)_R \times USp(2)_1 \times USp(2)$									
stack	N	$(n^1, l^1) \times (n^2, l^2) \times (n^3, l^3)$	$n_{\square\square}$	n_{\square}	b	b'	c	c'	1	4
a	8	$(-1, 1) \times (-1, 1) \times (-1, 1)$	0	4	0	3	3	-6	1	1
b	4	$(-2, 1) \times (0, 1) \times (-1, 1)$	-1	1	-	-	9	-10	1	0
c	4	$(-1, 2) \times (-1, 0) \times (5, 1)$	9	-9	-	-	-	-	0	1
1	2	$(1, 0) \times (1, 0) \times (2, 0)$	$x_A = 22x_B = 2x_C = \frac{11}{5}x_D$ $\beta_1^g = -3, \beta_4^g = -3$ $\chi_1 = \frac{1}{\sqrt{5}}, \chi_2 = \frac{11}{\sqrt{5}}, \chi_3 = 4\sqrt{5}$							
4	2	$(0, 1) \times (0, 1) \times (2, 0)$								

Using the same symmetry breaking method as processed for Model 2, we can obtain better gauge coupling relation closer to unification with $SU(2)_L$ gauge coupling suppressed for Model 3 to $SU(2)'_L$ gauge coupling relation in model 3-m, as shown in Table 14. Performing symmetry breaking to suppress the high $SU(2)_L$ gauge coupling first, will help to achieve gauge couplings unification via RGEs method as shown in the next section.

Table 14. D6-brane configurations and intersection numbers of Model 3-m, and its MSSM gauge coupling relation is $g_a^2 = \frac{24}{23}g_L^2 = \frac{13}{5}g_c^2 = \frac{65}{41}(\frac{5}{3}g_Y^2) = \frac{16}{5}\sqrt{3}\pi e^{\phi_4}$.

model 3-m	$U(4) \times U(2)_L \times U(2)_R \times USp(2)_1 \times USp(4)$									
stack	N	$(n^1, l^1) \times (n^2, l^2) \times (n^3, l^3)$	$n_{\square\square}$	n_{\square}	b	b'	c	c'	1	3
a	8	$(-1, 1) \times (-1, 0) \times (1, 1)$	0	0	3	0	-1	-2	0	0
b	4	$(-1, 4) \times (0, 1) \times (-1, 1)$	3	-3	-	-	-8	4	4	1
c	4	$(1, 0) \times (1, -1) \times (1, 3)$	-2	2	-	-	-	-	0	1
1	2	$(1, 0) \times (1, 0) \times (2, 0)$	$x_A = \frac{3}{4}x_B = \frac{1}{4}x_C = \frac{3}{4}x_D$ $\beta_1^g = -2, \beta_3^g = -4$ $\chi_1 = \frac{1}{2}, \chi_2 = \frac{3}{2}, \chi_3 = 1$							
3	4	$(0, 1) \times (1, 0) \times (0, 2)$								

4 Gauge Unification of Pati-Salam Generalization

With the above four classes of new supersymmetric Pati-Salam models obtained from generalized three-family of chiral fermion condition (represented by Model 1,2,3,4), and symmetry breaking mechanism introduced, here in this section we study whether the important gauge coupling unification presented in [54, 55] can still be realized. Before we discuss the string-scale gauge coupling unification in the current generalization, let's first review the basics to obtain gauge unification in supersymmetric Pati-Salam models from the former study.

In [54, 55], the string-scale gauge coupling relations were systematically investigated for all the independent 33 supersymmetric Pati-Salam models from the former searches.

With the decoupling of the exotic particles discussed, two-loop RGEs evolution methods are applied to approach string-scale gauge coupling relation by introducing different types of additional particles. These particles include additional particles from the adjoint representations of $SU(4)_C$ and $SU(2)_L$ gauge symmetries, SM vector-like particles from four-dimensional chiral sectors, and vector-like particles from $\mathcal{N} = 2$ subsector. In such a way, the total 33 independent supersymmetric Pati-Salam models all managed to arrive string-scale gauge coupling unification with the above additional particles introduced. Therefore, although these models do not directly have a traditional gauge coupling unification at string scale, an effective approach to realize the string-scale gauge coupling unification was established.

Recall that in the supersymmetric Pati-Salam models, $U(4)$ gauge symmetry arises from the a stack of D6-branes, while the $U(2)_L$ gauge symmetry and the $U(2)_R$ gauge symmetry arise from the b stack of D6-branes and c stack of D6-branes, respectively. The strong, weak and hypercharge gauge couplings g_a^2, g_b^2 and $\frac{5}{3}g_Y^2$ are constricted by the gauge coupling relation (3.11). As it has been mentioned in the introduction, to approach string-scale gauge coupling relation, RGEs evolution methods are often utilized [54, 59, 60]. In practice, at the two-loop level, the RGEs for the gauge couplings are presented in [56, 65–67]. Such that

$$\frac{d}{d \ln \mu} g_i = \frac{b_i}{(4\pi)^2} g_i^3 + \frac{g_i^3}{(4\pi)^4} \left[\sum_{j=1}^3 B_{ij} g_j^2 - \sum_{\alpha=u,d,e} d_i^\alpha \text{Tr} \left(h^{\alpha\dagger} h^\alpha \right) \right], \quad (4.1)$$

in which $g_i (i = 1, 2, 3)$ represents the SM gauge couplings, while the Yukawa couplings are represented by $h^\alpha (\alpha = u, d, e)$. And in SM the coefficients for the above beta functions are give in [68–71] as

$$b_{\text{SM}} = \left(\frac{41}{6} \frac{1}{k_Y}, -\frac{19}{6} \frac{1}{k_2}, -7 \right), \quad B_{\text{SM}} = \begin{pmatrix} \frac{199}{18} \frac{1}{k_Y^2} & \frac{27}{6} \frac{1}{k_Y k_2} & \frac{44}{3} \frac{1}{k_Y} \\ \frac{3}{2} \frac{1}{k_Y k_2} & \frac{35}{6} \frac{1}{k_2^2} & 12 \frac{1}{k_2} \\ \frac{11}{6} \frac{1}{k_Y} & \frac{9}{2} \frac{1}{k_2} & -26 \end{pmatrix}, \quad (4.2)$$

$$d_{\text{SM}}^u = \left(\frac{17}{6} \frac{1}{k_Y}, \frac{3}{2} \frac{1}{k_2}, 2 \right), \quad d_{\text{SM}}^d = 0, \quad d_{\text{SM}}^e = 0, \quad (4.3)$$

while in the supersymmetric models the coefficients are given in [72–74] by

$$b_{\text{SUSY}} = \left(11 \frac{1}{k_Y}, \frac{1}{k_2}, -3 \right), \quad B_{\text{SUSY}} = \begin{pmatrix} \frac{199}{9} \frac{1}{k_Y^2} & 9 \frac{1}{k_Y k_2} & \frac{88}{3} \frac{1}{k_Y} \\ 3 \frac{1}{k_Y k_2} & 25 \frac{1}{k_2^2} & 24 \frac{1}{k_2} \\ \frac{11}{3} \frac{1}{k_Y} & 9 \frac{1}{k_2} & 14 \end{pmatrix}, \quad (4.4)$$

$$d_{\text{SUSY}}^u = \left(\frac{26}{3} \frac{1}{k_Y}, 6 \frac{1}{k_2}, 4 \right), \quad d_{\text{SUSY}}^d = 0, \quad d_{\text{SUSY}}^e = 0, \quad (4.5)$$

in which k_Y and k_2 represent the general normalization factors.

4.1 String-scale Gauge Coupling Relations

In order to obtain the two-loop RGEs for SM gauge couplings, one-loop RGEs for Yukawa couplings need to be numerically studied with the new physics contributions and threshold considered [67].

To explore the renormalization group running of gauge couplings g_i from the Z-boson mass scale M_Z up to high energies, we numerically solve the two-loop RGEs for SM gauge couplings and one-loop RGEs for Yukawa couplings. The entire evolution is structured into three distinct stages, with each stage characterized by specific particle content and corresponding RGEs. In which, the first stage describes the coupling evolution from M_Z to the supersymmetry breaking scale M_S . Within this range, the particle spectrum is dominated by SM fields, such that the running of $g_i(\mu)$ is governed by the non-supersymmetric two-loop RGEs (4.2). The initial conditions at $\mu = M_Z$ are set by experimental measurements of SM gauge couplings,

$$g_1(M_Z) = \sqrt{k_Y} \frac{g_{em}}{\cos \theta_W}, \quad g_2(M_Z) = \sqrt{k_2} \frac{g_{em}}{\sin \theta_W}, \quad g_3(M_Z) = \sqrt{4\pi\alpha_s}. \quad (4.6)$$

Solving these RGEs yields the values of g_i at M_S , which serve as the boundary conditions for the subsequent supersymmetric evolution stage. Moving to the second stage from M_S to M_V , where M_V denotes the mass threshold of vector-like particles, the particle content expands to include SM superpartners. The running of gauge coupling is now dictated by the supersymmetric two-loop RGEs (4.4), which incorporate contributions from both SM fields and their superpartners. The third stage encompasses the energy interval $M_V \leq \mu \leq M_U$, where we extend the solution of supersymmetric RGEs to incorporate both one-loop and two-loop quantum corrections from the vector-like particles. Notably, the corrections from these vector-like particles modify the slope of $g_i(\mu)$ running, thereby driving the three gauge couplings toward mutual unification value to the scale M_U . By propagating $g_i(\mu)$ through the above three stages, we find that they converge to a unified value g_U at M_U .

The $SU(3)_C \times SU(2)_L \times U(1)_Y$ quantum numbers assigned to the vector-like particles

and their contributions to the one-loop beta functions [57, 66] are listed below.

$$XQ + \overline{XQ} = (\mathbf{3}, \mathbf{2}, \frac{1}{6}) + (\overline{\mathbf{3}}, \mathbf{2}, -\frac{1}{6}), \quad \Delta b = (\frac{1}{5}, 3, 2); \quad (4.7)$$

$$XU + \overline{XU} = (\mathbf{3}, \mathbf{1}, \frac{2}{3}) + (\overline{\mathbf{3}}, \mathbf{1}, -\frac{2}{3}), \quad \Delta b = (\frac{8}{5}, 0, 1); \quad (4.8)$$

$$XD + \overline{XD} = (\mathbf{3}, \mathbf{1}, -\frac{1}{3}) + (\overline{\mathbf{3}}, \mathbf{1}, \frac{1}{3}), \quad \Delta b = (\frac{2}{5}, 0, 1); \quad (4.9)$$

$$XL + \overline{XL} = (\mathbf{1}, \mathbf{2}, \frac{1}{2}) + (\mathbf{1}, \mathbf{2}, -\frac{1}{2}), \quad \Delta b = (\frac{3}{5}, 1, 0); \quad (4.10)$$

$$XE + \overline{XE} = (\mathbf{1}, \mathbf{1}, \mathbf{1}) + (\mathbf{1}, \mathbf{1}, -\mathbf{1}), \quad \Delta b = (\frac{6}{5}, 0, 0); \quad (4.11)$$

$$XG = (\mathbf{8}, \mathbf{1}, \mathbf{0}), \quad \Delta b = (0, 0, 3); \quad (4.12)$$

$$XW = (\mathbf{1}, \mathbf{3}, \mathbf{0}), \quad \Delta b = (0, 2, 0); \quad (4.13)$$

$$XT + \overline{XT} = (\mathbf{1}, \mathbf{3}, \mathbf{1}) + (\mathbf{1}, \mathbf{3}, -\mathbf{1}), \quad \Delta b = (\frac{18}{5}, 4, 0); \quad (4.14)$$

$$XS + \overline{XS} = (\mathbf{6}, \mathbf{1}, -\frac{2}{3}) + (\overline{\mathbf{6}}, \mathbf{1}, \frac{2}{3}), \quad \Delta b = (\frac{16}{5}, 0, 5); \quad (4.15)$$

$$XY + \overline{XY} = (\mathbf{3}, \mathbf{2}, -\frac{5}{6}) + (\overline{\mathbf{3}}, \mathbf{2}, \frac{5}{6}), \quad \Delta b = (5, 3, 2). \quad (4.16)$$

Following the formalism of [66], which provides a complete treatment of two-loop vector-like particle effects in SUSY models, we augment the supersymmetric RGEs (4.4) with these corrections. The full beta functions (4.1) governing the third stage of evolution thus incorporate both one- and two-loop contributions from the vector-like particles:

$$\beta_i = \beta_i^{(0)} + \beta_i^{(1, \text{VLP})} + \beta_i^{(2, \text{VLP})}, \quad (4.17)$$

where $\beta_i^{(0)}$ denotes the supersymmetric beta function following stage 2, and $\beta_i^{(1, \text{VLP})}$, $\beta_i^{(2, \text{VLP})}$ are the one- and two-loop vector-like particle induced corrections, respectively.

To be concrete, consider a vector-like quark pair $XQ + \overline{XQ}$, transforming as $(\mathbf{3}, \mathbf{2}, 1/6)$ under $SU(3)_C \times SU(2)_L \times U(1)_Y$. This pair contributes non-trivially to all three Δb_i coefficients, thereby depressing the running of each corresponding gauge coupling g_i . The degree of depression increases as Δb_i increases. That's to say, the inverse hypercharge coupling α^{-1} decreases more rapidly in models with the up-type vector-like quarks $XU + \overline{XU}$ than that in models with down-type vector-like quarks $XD + \overline{XD}$. Conversely, the $SU(3)_C$ adjoint XG is a singlet under $SU(2)_L \times U(1)_Y$, resulting in vanishing contributions $\Delta b_{1,2} = 0$. Consequently, while the running of g_1 and g_2 remains unchanged from Stage 2, the strong coupling g_3 is selectively adjusted by XG . This demonstrates how different vector-like particles can target specific gauge couplings, enabling precise tuning of the unification behavior.

4.2 Gauge Coupling Relation under Symmetry Breaking

Gauge coupling evolution requires well-defined initial conditions, vector-like particle content, and RGE structures. In this section, we specify these key points, consistent with experimental constraints and theoretical requirements.

Initial SM parameters at M_Z are fixed using experimental measurements [75–78], serving as boundary condition for stage 1 evolution from M_Z to M_S :

$$M_Z = 91.1876 \text{ GeV}, \quad m_t = 173.34 \pm 0.27(\text{stat}) \pm 0.71(\text{syst}) \text{ GeV}, \quad v = 174.10 \text{ GeV},$$

$$\alpha_s(M_Z) = 0.1179 \pm 0.0009, \quad \alpha_{em}^{-1}(M_Z) = 128.91 \pm 0.02, \quad \sin^2 \theta_W(M_Z) = 0.23122. \quad (4.18)$$

where M_Z is Z boson mass, m_t is top quark pole mass, v is Higgs vacuum expectation value, α_s is strong coupling constant, α_{em} is fine structure constant, and θ_W is weak mixing angle. The supersymmetric breaking scale $M_S \geq 1$ TeV is constrained by lower supersymmetric particle search bounds and gauge hierarchy preservation. Benchmark values 2.5 TeV or 3.0 TeV are tested: variations induce $< 5\%$ shifts in the unification scale M_U , with larger M_S lowering M_U . For consistency, $M_S = 3$ TeV is fixed.

Take Model 1, 2 and Model 3-m (with $SU(2)_L$ gauge coupling modified/suppressed by symmetry breaking) as examples, we study their gauge coupling relations at string scale as presented in figs. 1 to 3, in which the couplings are redefined as

$$\alpha_1 \equiv k_Y \frac{g_Y^2}{4\pi}, \quad \alpha_2 \equiv k_2 \frac{g_b^2}{4\pi}, \quad \alpha_3 \equiv k_3 \frac{g_a^2}{4\pi}. \quad (4.19)$$

where g_Y, g_b, g_a are bare couplings of $U(1)_Y, SU(2)_L, SU(3)_C$ and k_Y, k_2, k_3 are normalization factor. Take $k_3 = 1$, unification at M_U is defined as $\alpha_U^{-1} \equiv \alpha_1^{-1} = (\alpha_2^{-1} + \alpha_3^{-1})/2$, where α_U denotes the unified gauge coupling. The relative error $\Delta = |\alpha_1^{-1} - \alpha_2^{-1}|/\alpha_1^{-1}$ is limited to be less than 1.0%. For the evolution curves of $\alpha_i^{-1}(\mu)$ vs $\log_{10}(\mu)$, two distinct kinks emerge as hall mark features: the first arises at M_S due to the transition from non-supersymmetric to supersymmetric RGEs, while the second is induced at M_V due to the introduction of vector-like particle contributions. These kinks are experimentally testable in the future high-energy colliders.

For the first two models, we find that with normalized factor $k_Y < 1$ and $k_2 > 1$, the intersection of α_1^{-1} and α_3^{-1} curves lies above α_2^{-1} curve, preventing the unification of all three gauge couplings. To resolve this discrepancy and achieve the simultaneous intersection of α_i^{-1} at M_{string} , we introduce vector-like up-type/down-type quarks, $(XD + \overline{XD})$ or $(XU + \overline{XU})$, from the $\mathcal{N} = 2$ subsector. These particles transform as $(3, 1, 1/3)$ or $(3, 1, 2/3)$ under $SU(3)_C \times SU(2)_L \times U(1)_Y$, respectively, and their inclusion adjusts the beta functions governing coupling running. Specifically, their non-trivial quantum numbers contribute to Δb_1 and Δb_3 , while yielding $\Delta b_2 = 0$. This selective modification adjusts the slopes of the $U(1)$ and strong couplings relative to electroweak coupling, enabling the alignment of all three curves at M_{string} . Notably, the degree of slope adjustment depends on the number of vector-like particle pairs n_V and their masses M_V . Increasing n_V enhances the Δb_1 and Δb_3 corrections, while heavier M_V delays their impact until higher energy scales. By tuning these parameters, we numerically demonstrate the convergence of α_i^{-1} at M_{string} .

From brane construction, the number of vector-like particles $(XD + \overline{XD})$ and $(XU +$

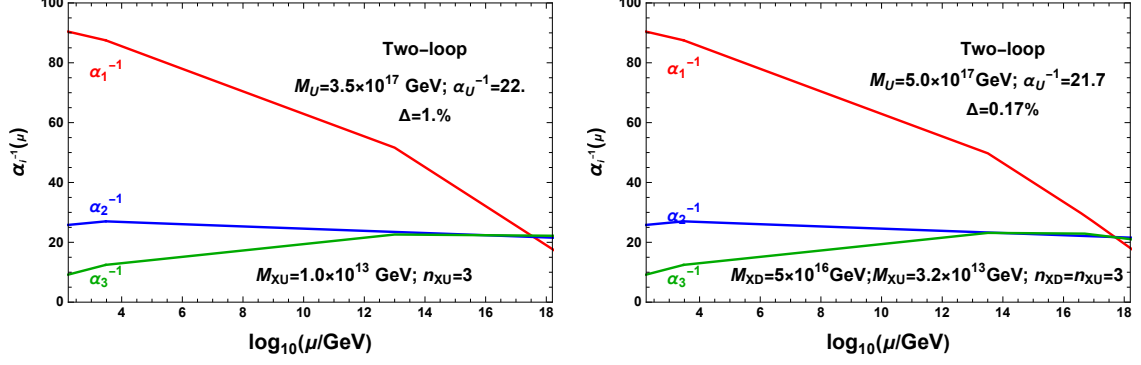


Figure 1. The evolution of two-loop gauge couplings in the Model 1 with vector-like particles (XU, \overline{XU}) and (XD, \overline{XD}) . The masses of these particles are set as $M_{XU} = 1.0 \times 10^{13}$ GeV (left panel) and $M_{XD} = 5 \times 10^{16}$ GeV, $M_{XU} = 3.2 \times 10^{13}$ GeV (right panel).

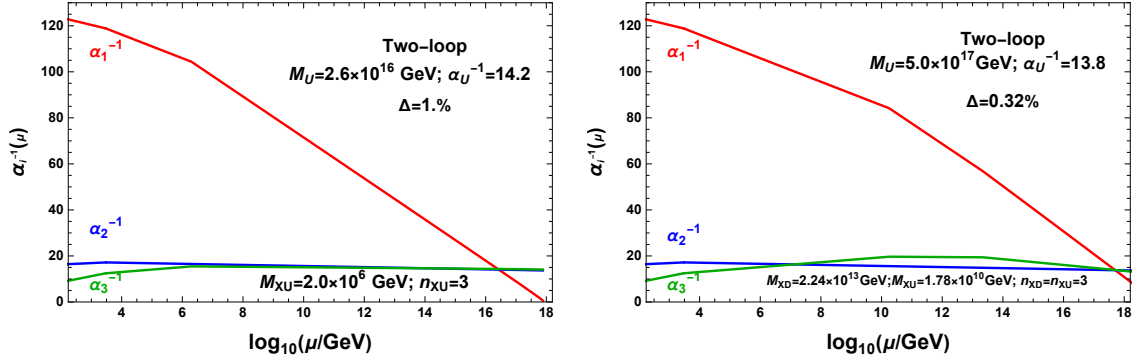


Figure 2. The evolution of two-loop gauge couplings in the Model 2 with vector-like particles (XU, \overline{XU}) and (XD, \overline{XD}) . The masses of these particles are set as $M_{XU} = 2.0 \times 10^6$ GeV (left panel) and $M_{XD} = 2.24 \times 10^{13}$ GeV, $M_{XU} = 1.78 \times 10^{10}$ GeV (right panel).

\overline{XU}) is determined by the intersection number I_{ac} of a - and c -brane stacks. For Models 1 and 2 (Tables 3 and 4), $I_{ac} = 3$, corresponding to three pairs of vector-like particles. After fine-tuning their masses, unification in Model 1 is achieved at $M_U = 3.5 \times 10^{17}$ GeV by introducing (XU, \overline{XU}) at $M_{XU} = 1.0 \times 10^{13}$ GeV. If both $(XD + \overline{XD})$ and $(XU + \overline{XU})$ are included, the precise string scale relation is achieved at $M_U = 5.0 \times 10^{17}$ GeV, with $M_{XD} = 5 \times 10^{16}$ GeV and $M_{XU} = 3.2 \times 10^{13}$ GeV. Moreover, three pairs of (XD, \overline{XD}) and (XU, \overline{XU}) can couple to the nine Higgs fields in the symmetric representation of $SU(2)_R$. The $SU(2)_R$ gauge symmetry is broken down to the $U(1)_{I_{3R}}$ gauge symmetry via D6-brane splitting, and then the Yukawa couplings for (XD, \overline{XD}) and (XU, \overline{XU}) can be different. If the Yukawa couplings for (XD, \overline{XD}) are about three orders larger than these for (XU, \overline{XU}) , we obtain the significant mass splittings between XD and XU . This mass splittings are crucial for achieving precise gauge coupling relation, as it allows independent tuning of the $U(1)$ and strong coupling across different energy scales.

For model 2, the factors $k_2 = 11/6$ and $k_Y = 5/14$ deviate significantly from 1, resulting in an initial value of electroweak coupling that lies very close to strong coupling at M_Z . Consequently, even with the inclusion of 3 (XU, \overline{XU}) pairs at $M_{XU} = 2.0 \times 10^6$

GeV, the unification scale remains slightly below the string scale, at $M_U = 2.6 \times 10^{16}$ GeV. To further push the unification energy scale toward M_{string} , we introduce additional (XD, \overline{XD}) pairs, which are integrated into the RGE evolution at two distinct thresholds $M_{XD} = 2.24 \times 10^{13}$ GeV and $M_{XU} = 1.78 \times 10^{10}$ GeV. As shown in the right panel of Figure 2, three kinks are visible in the α_1^{-1} and α_3^{-1} curves, corresponding to the successive integration of $(XD + \overline{XD})$ and (XU, \overline{XU}) . This multi-step inclusion enhances the Δ_1 and Δ_3 corrections above the corresponding thresholds, gradually adjusting the slopes of α_1^{-1} and α_3^{-1} . Through this hierarchical integration, we achieve precise gauge coupling at 5.0×10^{17} GeV.

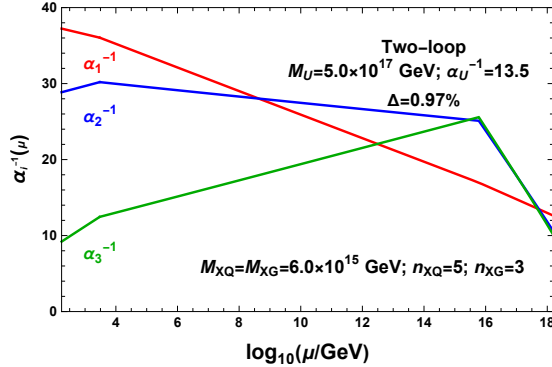


Figure 3. The evolution of two-loop gauge couplings in the Model 3-m with vector-like particles $5(XQ, \overline{XQ}) + 3XG$. The masses of these particles are set as $M_{XQ} = M_{XG} = 6.0 \times 10^{16}$ GeV.

In the case of Model 3, the large constant k_2 in the gauge coupling relation makes it difficult to achieve unification at the target energy scale through renormalization group running. Since $k_2 > 1$, this implies that at the unification scale the value of α_2^{-1} must be smaller than α_3^{-1} . Under renormalization group running, the curve of α_2^{-1} typically lies between those of α_1^{-1} and α_3^{-1} . It is very difficult to make it “drop” below the α_3^{-1} curve, let alone fall significantly lower.

Fortunately, stems from the canonical normalization requirement of the gauge kinetic terms get modified after symmetry breaking as we shown in Section 3.3. The $SU(2)_{L_1} \times SU(2)_{L_2}$ symmetry can be broken down to the diagonal subgroup $SU(2)_{L'}$ through the mechanism of vacuum expectation values. The coupling constant $g_{L'}$ of the resulting diagonal subgroup $SU(2)$ after symmetry breaking get suppressed which provides an alternative approach to achieve string-scale gauge coupling unification.

As shown in Table 14, with k_2 lowered via this approach, gauge coupling unification at the desired energy level becomes easier, with vector-like particles $(XQ + \overline{XQ})$ and XG with masses $M_{XQ} = M_{XG} = 6.0 \times 10^{16}$ introduced. The vector-like particles (XQ, \overline{XQ}) arise from the intersections between a and b stacks of D6-brane. Three chiral multiplets XG arise from aa sector of the adjoint representation of $SU(4)_C$. The number of introduced particle (XQ, \overline{XQ}) is determined by the intersection number of a - and b -brane stacks $I_{ab} = 5$, and therefore $n_{XQ} = 5$. From this approach, the slope of α_2^{-1} and α_3^{-1} are further suppressed than α_1^{-1} , and thus we achieve unification at string-scale, $M_U = 5.0 \times 10^{17}$ GeV.

Based on the above investigation, here we find the string-scale gauge coupling relation can be achieved at two-loop level via introducing the extra vector-like particles from $\mathcal{N} = 2$ subsector in these models. Furthermore, for the constructed models with large k_2 , by utilizing the symmetry breaking mechanism introduced in Section 3.3, we propose that the large k_2 can be highly suppressed and thus string-scale gauge coupling unification can be realized in a good manner as well. Again, the quantum numbers for these vector-like particles are the same as those of the SM fermions and their Hermitian conjugates. The number n_V of these particles is highly model dependent and can be determined from the corresponding brane intersection number. As discussed in Ref. [55], these additional particles can be decoupled through Higgs mechanism or instanton effects. With multiple pairs of extra particles emerge naturally, one only needs to fine-tune their masses to unify the gauge coupling near the string scale

$$M_U \sim M_{\text{string}} \simeq 5 \times 10^{17} \text{ GeV}. \quad (4.20)$$

To summarize, in our numerical check with symmetry breaking considered, we observe that the masses of these extra particles are determined by three factors: (i) the number of the particles, (ii) the beta functions and (iii) the precise energy scale where we realize the string-scale gauge coupling relations. Moreover, as n_V increase, the masses of these extra particles approach M_{string} .

5 Conclusions and Outlook

In this paper, realizing that the three-family of chiral fermion condition can actually be generalized from $I_{ab} + I_{ab'} = 3$; $I_{ac} = -3$, $I_{ac'} = 0$ (or $I_{ac} = 0$, $I_{ac'} = -3$) to $I_{ab} + I_{ab'} = 3$, $I_{ac} + I_{ac'} = -3$, we in particular searched for the new supersymmetric Pati-Salam models with the systematic algorithm built in [53]. While three generations of particles are realized by the brane intersection of a - and b/b' - stacks of branes, with $I_{ac} + I_{ac'} = -3$, four classes of new supersymmetric Pati-Salam models were obtained, represented by Model 1, 2, 3, 4. As follows, whether these new models arisen from the extended three-family of chiral fermions condition, such as $I_{ac} = 3$, $I_{ac'} = -6$ and $I_{ac} = -1$, $I_{ac'} = -2$, still preserve the string-scale gauge coupling unification are also investigated with symmetry breaking mechanism imposed.

Firstly, note that the three generation condition in supersymmetric Pati-Salam models can be extended and the three-family of chiral fermions can arise from different brane intersection, which further extend the landscape of $\mathcal{N} = 1$ supersymmetric Pati-Salam models that found in [53]. From the former investigation, these models are speculated to be very limited [10]. Nevertheless, in this paper we generalized the supersymmetric Pati-Salam models search to this scope. We in particular focused on the extended model building of supersymmetric Pati-Salam models from brane intersection. With the complete search method, we found there are four new classes of supersymmetric Pati-Salam models that were omitted under the former three generation condition. In precise, the three generation condition can provide three-family of chiral fermions with $I_{ac} = 3$, $I_{ac'} = -6$

and $I_{ac} = -1, I_{ac'} = -2$ as well. And for each above three generation condition, there are two classes of physical independent models, each with 6144 number of new supersymmetric Pati-Salam models found². These new models are in principle found via iteratively solving the Diophantine equations constituting of the new three generation conditions, RR tadpole cancellation conditions, and supersymmetry conditions. In each class, the supersymmetric Pati-Salam models have the same gauge coupling relation, while with distinct gauge coupling relations from the former investigation [53]. Take representative models from each class as example, we phenomenological studied the spectrum for each class. The Higgs multiples arise differently from the former investigations. In particular, these extended part of the supersymmetric Pati-Salam models are with rare filler branes, and maximally with two filler branes.

Secondly, consider the symmetry breaking method to suppress the $SU(2)_L$ gauge coupling, we show that the symmetry breaking mechanism helps to achieve string-scale gauge coupling relation at around M_{string} . This symmetry breaking mechanism is especially effective for models with high $k_2 = g_b^2/g_a^2$, that is often found to be difficult to realize gauge unification in RGEs evolution. Our key strategy is to introduce exotic vector-like particles to modify beta functions. We implement this strategy differently across models, matching exotic particles to each model's specific structure. For model 1 and 2, we introduce vector-like down-type quarks ($XD + \overline{XD}$) and up-type quarks ($XU + \overline{XU}$), both originating from the $\mathcal{N} = 2$ subsector. These particles give Δb_1 and Δb_3 corrections, adjusting the slopes of α_1^{-1} and α_3^{-1} to align with α_2^{-1} at M_{string} . For model 3-m, with symmetry breaking mechanism imposed, we introduce two complementary particles: vector-like quarks ($XQ + \overline{XQ}$) and a vector-like $SU(4)_C$ -adjoint particle XG . In particular, the vector-like particles (XQ, \overline{XQ}) arise from the intersections between a and b stacks of D6-brane. Three chiral multiplets XG arise from aa sector of the adjoint representation of $SU(4)_C$. Through two-loop RGE analysis, we demonstrate that these particles modify the beta functions to align all gauge couplings at M_{string} in supersymmetric Pati-Salam models studied.

Therefore, we proposed to extend the landscape of $\mathcal{N} = 1$ supersymmetric Pati-Salam models with the generalized three-family condition. And with symmetry breaking mechanism imposed, the revised RGE evolution were shown to realize the string-scale gauge coupling relation in an effective manner. Concrete models with string-scale gauge coupling relations achieved for new supersymmetric Pati-Salam models were presented.

For future investigation, we think it will be interesting and worthwhile to study the general three-family of chiral fermion condition, especially in brane intersection models. Although it was shown to be very difficult to realize these models as they are highly constraint by brane intersection, with the complete search method constructed in [53] these models can be effectively found. And imposing symmetry breaking mechanism before the RGE evolution provides an effective approach to realize string-scale gauge coupling relation in brane intersection theories. This provides a robust mechanism for resolving the scale mismatch between GUTs and string theory in generic intersecting D-brane constructions.

²Examples of these new supersymmetric Pati-Salam models with duality variations are presented in the Appendix.

Acknowledgments

We acknowledge Haotian Huang-fu for useful discussion. TL is supported in part by the National Key Research and Development Program of China Grant No. 2020YFC2201504, by the Projects No. 11875062, No. 11947302, No. 12047503, and No. 12275333 supported by the National Natural Science Foundation of China, by the Key Research Program of the Chinese Academy of Sciences, Grant No. XDPB15, by the Scientific Instrument Developing Project of the Chinese Academy of Sciences, Grant No. YJKYYQ20190049, by the International Partnership Program of Chinese Academy of Sciences for Grand Challenges, Grant No. 112311KYSB20210012, and by the Henan Province Outstanding Foreign Scientist Studio Project, No.GZS2025008. RS is supported by the Fundamental Research Funds for the Central Universities Grant No. E4EQ0102X2. LW is supported by the Natural Science Basic Research Program of Shaanxi, Grant No. 2024JC-YBMS-039.

References

- [1] M. Cvetič, M. Plumacher, and J. Wang, *Three family type IIB orientifold string vacua with nonAbelian Wilson lines*, *JHEP* **04** (2000) 004, [[hep-th/9911021](#)].
- [2] M. Berkooz, M. R. Douglas, and R. G. Leigh, *Branes intersecting at angles*, *Nucl. Phys. B* **480** (1996) 265–278, [[hep-th/9606139](#)].
- [3] G. Aldazabal, L. E. Ibanez, F. Quevedo, and A. M. Uranga, *D-branes at singularities: A Bottom up approach to the string embedding of the standard model*, *JHEP* **08** (2000) 002, [[hep-th/0005067](#)].
- [4] G. Aldazabal, S. Franco, L. E. Ibanez, R. Rabadan, and A. M. Uranga, *Intersecting brane worlds*, *JHEP* **02** (2001) 047, [[hep-ph/0011132](#)].
- [5] G. Aldazabal, S. Franco, L. E. Ibanez, R. Rabadan, and A. M. Uranga, *$D = 4$ chiral string compactifications from intersecting branes*, *J. Math. Phys.* **42** (2001) 3103–3126, [[hep-th/0011073](#)].
- [6] L. E. Ibanez, F. Marchesano, and R. Rabadan, *Getting just the standard model at intersecting branes*, *JHEP* **11** (2001) 002, [[hep-th/0105155](#)].
- [7] M. Cvetič, G. Shiu, and A. M. Uranga, *Three family supersymmetric standard - like models from intersecting brane worlds*, *Phys. Rev. Lett.* **87** (2001) 201801, [[hep-th/0107143](#)].
- [8] R. Blumenhagen, L. Gorlich, and T. Ott, *Supersymmetric intersecting branes on the type 2A $T6 / Z(4)$ orientifold*, *JHEP* **01** (2003) 021, [[hep-th/0211059](#)].
- [9] M. Cvetič, A. M. Uranga, and J. Wang, *Discrete Wilson lines in $N=1$ $D = 4$ type IIB orientifolds: A Systematic exploration for $Z(6)$ orientifold*, *Nucl. Phys. B* **595** (2001) 63–92, [[hep-th/0010091](#)].
- [10] M. Cvetič, T. Li, and T. Liu, *Supersymmetric Pati-Salam models from intersecting $D6$ -branes: A Road to the standard model*, *Nucl. Phys. B* **698** (2004) 163–201, [[hep-th/0403061](#)].
- [11] C. M. Chen, G. V. Kraniotis, V. E. Mayes, D. V. Nanopoulos, and J. W. Walker, *A Supersymmetric flipped $SU(5)$ intersecting brane world*, *Phys. Lett. B* **611** (2005) 156–166, [[hep-th/0501182](#)].

- [12] R. Blumenhagen, M. Cvetič, P. Langacker, and G. Shiu, *Toward realistic intersecting D-brane models*, *Ann. Rev. Nucl. Part. Sci.* **55** (2005) 71–139, [[hep-th/0502005](#)].
- [13] C.-M. Chen, T. Li, V. E. Mayes, and D. V. Nanopoulos, *Variations of the hidden sector in a realistic intersecting brane model*, *J. Phys. G* **35** (2008) 095008, [[arXiv:0704.1855](#)].
- [14] J. D. Lykken, E. Poppitz, and S. P. Trivedi, *Branes with GUTs and supersymmetry breaking*, *Nucl. Phys. B* **543** (1999) 105–121, [[hep-th/9806080](#)].
- [15] G. Honecker and J. Vanhoof, *Yukawa couplings and masses of non-chiral states for the Standard Model on D6-branes on $T6/Z6'$* , *JHEP* **04** (2012) 085, [[arXiv:1201.3604](#)].
- [16] G. Honecker, I. Koltermann, and W. Staessens, *Deformations, Moduli Stabilisation and Gauge Couplings at One-Loop*, *JHEP* **04** (2017) 023, [[arXiv:1702.08424](#)].
- [17] P. Anastasopoulos, T. P. T. Dijkstra, E. Kiritsis, and A. N. Schellekens, *Orientifolds, hypercharge embeddings and the Standard Model*, *Nucl. Phys. B* **759** (2006) 83–146, [[hep-th/0605226](#)].
- [18] P. Anastasopoulos, E. Kiritsis, and A. Lionetto, *On mass hierarchies in orientifold vacua*, *JHEP* **08** (2009) 026, [[arXiv:0905.3044](#)].
- [19] P. Anastasopoulos, G. K. Leontaris, and N. D. Vlachos, *Phenomenological Analysis of D-Brane Pati-Salam Vacua*, *JHEP* **05** (2010) 011, [[arXiv:1002.2937](#)].
- [20] P. Anastasopoulos, G. K. Leontaris, R. Richter, and A. N. Schellekens, *$SU(5)$ D-brane realizations, Yukawa couplings and proton stability*, *JHEP* **12** (2010) 011, [[arXiv:1010.5188](#)].
- [21] P. Anastasopoulos, G. K. Leontaris, R. Richter, and A. N. Schellekens, *Avoiding disastrous couplings in $SU(5)$ orientifolds*, *Fortsch. Phys.* **59** (2011) 1144–1148.
- [22] J. Ecker, G. Honecker, and W. Staessens, *D6-brane model building on $\mathbb{Z}_2 \times \mathbb{Z}_6$: MSSM-like and left–right symmetric models*, *Nucl. Phys. B* **901** (2015) 139–215, [[arXiv:1509.00048](#)].
- [23] F. Marchesano, B. Schellekens, and T. Weigand, *D-brane and F-theory Model Building*. 2024. [[arXiv:2212.07443](#)].
- [24] I. Antoniadis and S. Dimopoulos, *Splitting supersymmetry in string theory*, *Nucl. Phys. B* **715** (2005) 120–140, [[hep-th/0411032](#)].
- [25] I. Antoniadis, *Aspects of string phenomenology*, *Int. J. Mod. Phys. A* **25** (2010) 4727–4740.
- [26] E. Kiritsis, *Orientifolds, and the search for the standard model in string theory*, *Les Houches* **87** (2008) 45–123.
- [27] E. Kiritsis, *D-branes in standard model building, gravity and cosmology*, *Phys. Rept.* **421** (2005) 105–190, [[hep-th/0310001](#)]. [Erratum: *Phys.Rept.* 429, 121–122 (2006)].
- [28] I. Brunner, K. Hori, K. Hosomichi, and J. Walcher, *Orientifolds of Gepner models*, *JHEP* **02** (2007) 001, [[hep-th/0401137](#)].
- [29] J. R. Ellis, S. Kelley, and D. V. Nanopoulos, *Probing the desert using gauge coupling unification*, *Phys. Lett. B* **260** (1991) 131–137.
- [30] P. Langacker and M.-x. Luo, *Implications of precision electroweak experiments for M_t , ρ_0 , $\sin^2 \theta_W$ and grand unification*, *Phys. Rev. D* **44** (1991) 817–822.
- [31] U. Amaldi, W. de Boer, and H. Furstenuau, *Comparison of grand unified theories with electroweak and strong coupling constants measured at LEP*, *Phys. Lett. B* **260** (1991) 447–455.

- [32] K. R. Dienes, *String theory and the path to unification: A Review of recent developments*, *Phys. Rept.* **287** (1997) 447–525, [[hep-th/9602045](#)].
- [33] C.-M. Chen, T. Li, V. E. Mayes, and D. V. Nanopoulos, *A Realistic world from intersecting D6-branes*, *Phys. Lett. B* **665** (2008) 267–270, [[hep-th/0703280](#)].
- [34] C.-M. Chen, T. Li, V. E. Mayes, and D. V. Nanopoulos, *Towards realistic supersymmetric spectra and Yukawa textures from intersecting branes*, *Phys. Rev. D* **77** (2008) 125023, [[arXiv:0711.0396](#)].
- [35] M. Cvetič and I. Papadimitriou, *More supersymmetric standard - like models from intersecting D6-branes on type IIA orientifolds*, *Phys. Rev. D* **67** (2003) 126006, [[hep-th/0303197](#)].
- [36] M. Cvetič, I. Papadimitriou, and G. Shiu, *Supersymmetric three family SU(5) grand unified models from type IIA orientifolds with intersecting D6-branes*, *Nucl. Phys. B* **659** (2003) 193–223, [[hep-th/0212177](#)]. [Erratum: *Nucl.Phys.B* 696, 298–298 (2004)].
- [37] M. Cvetič, P. Langacker, and G. Shiu, *Phenomenology of a three family standard like string model*, *Phys. Rev. D* **66** (2002) 066004, [[hep-ph/0205252](#)].
- [38] M. Cvetič, P. Langacker, and G. Shiu, *A Three family standard - like orientifold model: Yukawa couplings and hierarchy*, *Nucl. Phys. B* **642** (2002) 139–156, [[hep-th/0206115](#)].
- [39] M. Cvetič, P. Langacker, and J. Wang, *Dynamical Supersymmetry Breaking in Standard - Like Models with Intersecting D6-Branes*, *Phys. Rev. D* **68** (2003) 046002, [[hep-th/0303208](#)].
- [40] M. Cvetič and I. Papadimitriou, *Conformal field theory couplings for intersecting D-branes on orientifolds*, *Phys. Rev. D* **68** (2003) 046001, [[hep-th/0303083](#)]. [Erratum: *Phys.Rev.D* 70, 029903 (2004)].
- [41] G. Honecker, *Chiral supersymmetric models on an orientifold of $Z(4) \times Z(2)$ with intersecting D6-branes*, *Nucl. Phys. B* **666** (2003) 175–196, [[hep-th/0303015](#)].
- [42] C.-M. Chen, T. Li, and D. V. Nanopoulos, *Standard-like model building on Type II orientifolds*, *Nucl. Phys. B* **732** (2006) 224–242, [[hep-th/0509059](#)].
- [43] M. R. Douglas and W. Taylor, *The Landscape of intersecting brane models*, *JHEP* **01** (2007) 031, [[hep-th/0606109](#)].
- [44] J. Halverson, B. Nelson, and F. Ruehle, *Branes with Brains: Exploring String Vacua with Deep Reinforcement Learning*, *JHEP* **06** (2019) 003, [[arXiv:1903.11616](#)].
- [45] G. J. Loges and G. Shiu, *Breeding Realistic D-Brane Models*, *Fortsch. Phys.* **70** (2022), no. 5 2200038, [[arXiv:2112.08391](#)].
- [46] G. J. Loges and G. Shiu, *134 billion intersecting brane models*, *JHEP* **12** (2022) 097, [[arXiv:2206.03506](#)].
- [47] M. Cvetič, P. Langacker, T.-j. Li, and T. Liu, *D6-brane splitting on type IIA orientifolds*, *Nucl. Phys. B* **709** (2005) 241–266, [[hep-th/0407178](#)].
- [48] M. Cvetič, G. Shiu, and A. M. Uranga, *Chiral four-dimensional N=1 supersymmetric type 2A orientifolds from intersecting D6 branes*, *Nucl. Phys. B* **615** (2001) 3–32, [[hep-th/0107166](#)].
- [49] T. Li, A. Mansha, and R. Sun, *Revisiting the supersymmetric Pati–Salam models from intersecting D6-branes*, *Eur. Phys. J. C* **81** (2021), no. 1 82, [[arXiv:1910.04530](#)].
- [50] T. Li, A. Mansha, R. Sun, L. Wu, and W. He, *N=1 supersymmetric $SU(12)_C \times SU(2)_L \times SU(2)_R$ models, $SU(4)_C \times SU(6)_L \times SU(2)_R$ models, and*

- $SU(4)_C \times SU(2)_L \times SU(6)_R$ models from intersecting D6-branes, *Phys. Rev. D* **104** (2021), no. 4 046018.
- [51] T. Li, A. Mansha, and R. Sun, *Generalized Supersymmetric Pati-Salam Models from Intersecting D6-branes*, [arXiv:1912.11633](#).
- [52] T. Li, R. Sun, and C. Zhang, *Four-family supersymmetric Pati-Salam models from intersecting D6-branes*, *Commun. Theor. Phys.* **74** (2022), no. 6 065201, [[arXiv:2202.10252](#)].
- [53] W. He, T. Li, and R. Sun, *The complete search for the supersymmetric Pati-Salam models from intersecting D6-branes*, *JHEP* **08** (2022) 044, [[arXiv:2112.09632](#)].
- [54] W. He, T. Li, R. Sun, and L. Wu, *The final model building for the supersymmetric Pati-Salam models from intersecting D6-branes*, *Eur. Phys. J. C* **82** (2022), no. 8 710, [[arXiv:2112.09630](#)].
- [55] T. Li, R. Sun, and L. Wu, *String-scale gauge coupling relations in the supersymmetric Pati-Salam models from intersecting D6-branes*, *JHEP* **03** (2023) 210, [[arXiv:2212.05875](#)].
- [56] V. Barger, J. Jiang, P. Langacker, and T. Li, *Non-canonical gauge coupling unification in high-scale supersymmetry breaking*, *Nucl. Phys. B* **726** (2005) 149–170, [[hep-ph/0504093](#)].
- [57] J. Jiang, T. Li, and D. V. Nanopoulos, *Testable Flipped $SU(5) \times U(1)(X)$ Models*, *Nucl. Phys. B* **772** (2007) 49–66, [[hep-ph/0610054](#)].
- [58] J. Jiang, T. Li, D. V. Nanopoulos, and D. Xie, *F-SU(5)*, *Phys. Lett. B* **677** (2009) 322–325, [[arXiv:0811.2807](#)].
- [59] H.-Y. Chen, I. Gogoladze, S. Hu, T. Li, and L. Wu, *The Minimal GUT with Inflaton and Dark Matter Unification*, *Eur. Phys. J. C* **78** (2018), no. 1 26, [[arXiv:1703.07542](#)].
- [60] H.-Y. Chen, I. Gogoladze, S. Hu, T. Li, and L. Wu, *Natural Higgs Inflation, Gauge Coupling Unification, and Neutrino Masses*, *Int. J. Mod. Phys. A* **35** (2020), no. 21 2050117, [[arXiv:1805.00161](#)].
- [61] R. Blumenhagen, B. Kors, and D. Lust, *Type I strings with F flux and B flux*, *JHEP* **02** (2001) 030, [[hep-th/0012156](#)].
- [62] T. R. Taylor, *Dilaton, gaugino condensation and supersymmetry breaking*, *Phys. Lett. B* **252** (1990) 59–62.
- [63] R. Brustein and P. J. Steinhardt, *Challenges for superstring cosmology*, *Phys. Lett. B* **302** (1993) 196–201, [[hep-th/9212049](#)].
- [64] B. de Carlos, J. A. Casas, and C. Munoz, *Supersymmetry breaking and determination of the unification gauge coupling constant in string theories*, *Nucl. Phys. B* **399** (1993) 623–653, [[hep-th/9204012](#)].
- [65] V. Barger, C.-W. Chiang, J. Jiang, and T. Li, *Axion models with high-scale supersymmetry breaking*, *Nucl. Phys. B* **705** (2005) 71–91, [[hep-ph/0410252](#)].
- [66] V. Barger, N. G. Deshpande, J. Jiang, P. Langacker, and T. Li, *Implications of Canonical Gauge Coupling Unification in High-Scale Supersymmetry Breaking*, *Nucl. Phys. B* **793** (2008) 307–325, [[hep-ph/0701136](#)].
- [67] I. Gogoladze, B. He, and Q. Shafi, *New Fermions at the LHC and Mass of the Higgs Boson*, *Phys. Lett. B* **690** (2010) 495–500, [[arXiv:1004.4217](#)].

- [68] M. E. Machacek and M. T. Vaughn, *Two Loop Renormalization Group Equations in a General Quantum Field Theory. 1. Wave Function Renormalization*, *Nucl. Phys. B* **222** (1983) 83–103.
- [69] M. E. Machacek and M. T. Vaughn, *Two Loop Renormalization Group Equations in a General Quantum Field Theory. 2. Yukawa Couplings*, *Nucl. Phys. B* **236** (1984) 221–232.
- [70] M. E. Machacek and M. T. Vaughn, *Two Loop Renormalization Group Equations in a General Quantum Field Theory. 3. Scalar Quartic Couplings*, *Nucl. Phys. B* **249** (1985) 70–92.
- [71] G. Cvetič, C. S. Kim, and S. S. Hwang, *Higgs mediated flavor changing neutral currents in the general framework with two Higgs doublets: An RGE analysis*, *Phys. Rev. D* **58** (1998) 116003, [[hep-ph/9806282](#)].
- [72] V. D. Barger, M. S. Berger, and P. Ohmann, *Supersymmetric grand unified theories: Two loop evolution of gauge and Yukawa couplings*, *Phys. Rev. D* **47** (1993) 1093–1113, [[hep-ph/9209232](#)].
- [73] V. D. Barger, M. S. Berger, and P. Ohmann, *The Supersymmetric particle spectrum*, *Phys. Rev. D* **49** (1994) 4908–4930, [[hep-ph/9311269](#)].
- [74] S. P. Martin and M. T. Vaughn, *Two loop renormalization group equations for soft supersymmetry breaking couplings*, *Phys. Rev. D* **50** (1994) 2282, [[hep-ph/9311340](#)]. [Erratum: *Phys.Rev.D* 78, 039903 (2008)].
- [75] **Particle Data Group** Collaboration, M. Tanabashi et al., *Review of Particle Physics*, *Phys. Rev. D* **98** (2018), no. 3 030001.
- [76] **Particle Data Group** Collaboration, P. A. Zyla et al., *Review of Particle Physics*, *PTEP* **2020** (2020), no. 8 083C01.
- [77] **ATLAS, CDF, CMS, D0** Collaboration, *First combination of Tevatron and LHC measurements of the top-quark mass*, [arXiv:1403.4427](#).
- [78] D. d’Enterria et al., *The strong coupling constant: state of the art and the decade ahead*, *J. Phys. G* **51** (2024), no. 9 090501, [[arXiv:2203.08271](#)].

A Generalized Supersymmetric Pati-Salam Models

In this section, we present some other examples of new supersymmetric Pati-Salam models from the three-family generalization, which are related to Model 1 (Table 15-24), Model 2 (Table 25-34), Model 3 (Table 35-44), Model 4 (Table 45-54), respectively. These new supersymmetric Pati-Salam models with the same MSSM gauge coupling relation are related by symmetry transformations, such as, D6-brane Sign Equivalent Principle (DSEP), Type I and II T-dualities, as discussed in [10, 53].

Table 15. D6-brane configurations and intersection numbers of Model 5, and its MSSM gauge coupling relation is $g_a^2 = \frac{7}{6}g_b^2 = \frac{35}{66}g_c^2 = \frac{175}{268}(\frac{5}{3}g_Y^2) = \frac{8\sqrt[4]{25^3}\pi e^{\phi_4}}{11\sqrt{3}}$.

model 5	$U(4) \times U(2)_L \times U(2)_R \times USp(2)$								
stack	N	$(n^1, l^1) \times (n^2, l^2) \times (n^3, l^3)$	$n_{\square\square}$	n_{\square}	b	b'	c	c'	1
a	8	$(1, 1) \times (1, 0) \times (1, -1)$	0	0	3	0	-6	3	0
b	4	$(1, -1) \times (1, -1) \times (1, 2)$	-2	-6	-	-	0	8	2
c	4	$(1, 5) \times (0, 1) \times (-1, -2)$	-9	9	-	-	-	-	10
1	2	$(1, 0) \times (1, 0) \times (2, 0)$	$x_A = \frac{1}{12}x_B = \frac{1}{10}x_C = \frac{1}{12}x_D$ $\beta_1^g = 6$ $\chi_1 = \frac{1}{\sqrt{10}}, \chi_2 = \frac{\sqrt{\frac{5}{2}}}{6}, \chi_3 = \sqrt{\frac{2}{5}}$						

Table 16. D6-brane configurations and intersection numbers of Model 6, and its MSSM gauge coupling relation is $g_a^2 = \frac{7}{6}g_b^2 = \frac{35}{66}g_c^2 = \frac{175}{268}(\frac{5}{3}g_Y^2) = \frac{8\sqrt[4]{25^3}\pi e^{\phi_4}}{11\sqrt{3}}$.

model 6	$U(4) \times U(2)_L \times U(2)_R \times USp(2)$								
stack	N	$(n^1, l^1) \times (n^2, l^2) \times (n^3, l^3)$	$n_{\square\square}$	n_{\square}	b	b'	c	c'	1
a	8	$(1, 1) \times (1, 0) \times (1, -1)$	0	0	3	0	-6	3	0
b	4	$(1, -1) \times (1, -1) \times (1, 2)$	-2	-6	-	-	0	8	2
c	4	$(-1, -5) \times (0, 1) \times (1, 2)$	-9	9	-	-	-	-	10
1	2	$(1, 0) \times (1, 0) \times (2, 0)$	$x_A = \frac{1}{12}x_B = \frac{1}{10}x_C = \frac{1}{12}x_D$ $\beta_1^g = 6$ $\chi_1 = \frac{1}{\sqrt{10}}, \chi_2 = \frac{\sqrt{\frac{5}{2}}}{6}, \chi_3 = \sqrt{\frac{2}{5}}$						

Table 17. D6-brane configurations and intersection numbers of Model 7, and its MSSM gauge coupling relation is $g_a^2 = \frac{7}{6}g_b^2 = \frac{35}{66}g_c^2 = \frac{175}{268}(\frac{5}{3}g_Y^2) = \frac{8\sqrt[4]{25^3}\pi e^{\phi_4}}{11\sqrt{3}}$.

model 7	$U(4) \times U(2)_L \times U(2)_R \times USp(2)$								
stack	N	$(n^1, l^1) \times (n^2, l^2) \times (n^3, l^3)$	$n_{\square\square}$	n_{\square}	b	b'	c	c'	1
a	8	$(1, 1) \times (1, 0) \times (1, -1)$	0	0	3	0	3	-6	0
b	4	$(1, -1) \times (1, -1) \times (1, 2)$	-2	-6	-	-	8	0	2
c	4	$(1, -5) \times (0, 1) \times (1, -2)$	9	-9	-	-	-	-	10
1	2	$(1, 0) \times (1, 0) \times (2, 0)$	$x_A = \frac{1}{12}x_B = \frac{1}{10}x_C = \frac{1}{12}x_D$ $\beta_1^g = 6$ $\chi_1 = \frac{1}{\sqrt{10}}, \chi_2 = \frac{\sqrt{\frac{5}{2}}}{6}, \chi_3 = \sqrt{\frac{2}{5}}$						

Table 18. D6-brane configurations and intersection numbers of Model 8, and its MSSM gauge coupling relation is $g_a^2 = \frac{7}{6}g_b^2 = \frac{35}{66}g_c^2 = \frac{175}{268}(\frac{5}{3}g_Y^2) = \frac{8\sqrt[4]{25^3}\pi e^{\phi_4}}{11\sqrt{3}}$.

model 8	$U(4) \times U(2)_L \times U(2)_R \times USp(2)$								
stack	N	$(n^1, l^1) \times (n^2, l^2) \times (n^3, l^3)$	$n_{\square\square}$	n_{\square}	b	b'	c	c'	1
a	8	$(1, 1) \times (1, 0) \times (1, -1)$	0	0	3	0	-6	3	0
b	4	$(1, -1) \times (1, -1) \times (1, 2)$	-2	-6	-	-	0	8	2
c	4	$(1, 5) \times (0, -1) \times (1, 2)$	-9	9	-	-	-	-	10
1	2	$(1, 0) \times (1, 0) \times (2, 0)$	$x_A = \frac{1}{12}x_B = \frac{1}{10}x_C = \frac{1}{12}x_D$ $\beta_1^g = 6$ $\chi_1 = \frac{1}{\sqrt{10}}, \chi_2 = \frac{\sqrt{\frac{5}{2}}}{6}, \chi_3 = \sqrt{\frac{2}{5}}$						

Table 19. D6-brane configurations and intersection numbers of Model 9, and its MSSM gauge coupling relation is $g_a^2 = \frac{7}{6}g_b^2 = \frac{35}{66}g_c^2 = \frac{175}{268}(\frac{5}{3}g_Y^2) = \frac{8\sqrt[4]{25^3}\pi e^{\phi_4}}{11\sqrt{3}}$.

model 9	$U(4) \times U(2)_L \times U(2)_R \times USp(2)$								
stack	N	$(n^1, l^1) \times (n^2, l^2) \times (n^3, l^3)$	$n_{\square\square}$	n_{\square}	b	b'	c	c'	1
a	8	$(1, 1) \times (1, 0) \times (1, -1)$	0	0	3	0	3	-6	0
b	4	$(1, -1) \times (1, -1) \times (1, 2)$	-2	-6	-	-	8	0	2
c	4	$(-1, 5) \times (0, -1) \times (1, -2)$	9	-9	-	-	-	-	10
1	2	$(1, 0) \times (1, 0) \times (2, 0)$	$x_A = \frac{1}{12}x_B = \frac{1}{10}x_C = \frac{1}{12}x_D$ $\beta_1^g = 6$ $\chi_1 = \frac{1}{\sqrt{10}}, \chi_2 = \frac{\sqrt{\frac{5}{2}}}{6}, \chi_3 = \sqrt{\frac{2}{5}}$						

Table 20. D6-brane configurations and intersection numbers of Model 10, and its MSSM gauge coupling relation is $g_a^2 = \frac{7}{6}g_b^2 = \frac{35}{66}g_c^2 = \frac{175}{268}(\frac{5}{3}g_Y^2) = \frac{8\sqrt[4]{25^3}\pi e^{\phi_4}}{11\sqrt{3}}$.

model 10	$U(4) \times U(2)_L \times U(2)_R \times USp(2)$								
stack	N	$(n^1, l^1) \times (n^2, l^2) \times (n^3, l^3)$	$n_{\square\square}$	n_{\square}	b	b'	c	c'	1
a	8	$(1, 1) \times (1, 0) \times (1, -1)$	0	0	3	0	3	-6	0
b	4	$(1, -1) \times (1, -1) \times (1, 2)$	-2	-6	-	-	8	0	2
c	4	$(1, -5) \times (0, -1) \times (-1, 2)$	9	-9	-	-	-	-	10
1	2	$(1, 0) \times (1, 0) \times (2, 0)$	$x_A = \frac{1}{12}x_B = \frac{1}{10}x_C = \frac{1}{12}x_D$ $\beta_1^g = 6$ $\chi_1 = \frac{1}{\sqrt{10}}, \chi_2 = \frac{\sqrt{\frac{5}{2}}}{6}, \chi_3 = \sqrt{\frac{2}{5}}$						

Table 21. D6-brane configurations and intersection numbers of Model 11, and its MSSM gauge coupling relation is $g_a^2 = \frac{7}{6}g_b^2 = \frac{35}{66}g_c^2 = \frac{175}{268}(\frac{5}{3}g_Y^2) = \frac{8\sqrt[4]{25^{3/4}}\pi e^{\phi_4}}{11\sqrt{3}}$.

model 11	$U(4) \times U(2)_L \times U(2)_R \times USp(2)$								
stack	N	$(n^1, l^1) \times (n^2, l^2) \times (n^3, l^3)$	$n_{\square\square}$	n_{\square}	b	b'	c	c'	1
a	8	$(1, 1) \times (1, 0) \times (1, -1)$	0	0	3	0	-6	3	0
b	4	$(1, -1) \times (1, -1) \times (1, 2)$	-2	-6	-	-	0	8	2
c	4	$(-1, -5) \times (0, -1) \times (-1, -2)$	-9	9	-	-	-	-	10
1	2	$(1, 0) \times (1, 0) \times (2, 0)$	$x_A = \frac{1}{12}x_B = \frac{1}{10}x_C = \frac{1}{12}x_D$ $\beta_1^g = 6$ $\chi_1 = \frac{1}{\sqrt{10}}, \chi_2 = \frac{\sqrt{\frac{5}{2}}}{6}, \chi_3 = \sqrt{\frac{2}{5}}$						

Table 22. D6-brane configurations and intersection numbers of Model 12, and its MSSM gauge coupling relation is $g_a^2 = \frac{7}{6}g_b^2 = \frac{35}{66}g_c^2 = \frac{175}{268}(\frac{5}{3}g_Y^2) = \frac{8\sqrt[4]{25^{3/4}}\pi e^{\phi_4}}{11\sqrt{3}}$.

model 12	$U(4) \times U(2)_L \times U(2)_R \times USp(2)$								
stack	N	$(n^1, l^1) \times (n^2, l^2) \times (n^3, l^3)$	$n_{\square\square}$	n_{\square}	b	b'	c	c'	1
a	8	$(1, 1) \times (1, 0) \times (1, -1)$	0	0	0	3	3	-6	0
b	4	$(1, 1) \times (1, 1) \times (1, -2)$	2	6	-	-	0	-8	2
c	4	$(-1, 5) \times (0, 1) \times (-1, 2)$	9	-9	-	-	-	-	10
1	2	$(1, 0) \times (1, 0) \times (2, 0)$	$x_A = \frac{1}{12}x_B = \frac{1}{10}x_C = \frac{1}{12}x_D$ $\beta_1^g = 6$ $\chi_1 = \frac{1}{\sqrt{10}}, \chi_2 = \frac{\sqrt{\frac{5}{2}}}{6}, \chi_3 = \sqrt{\frac{2}{5}}$						

Table 23. D6-brane configurations and intersection numbers of Model 13, and its MSSM gauge coupling relation is $g_a^2 = \frac{7}{6}g_b^2 = \frac{35}{66}g_c^2 = \frac{175}{268}(\frac{5}{3}g_Y^2) = \frac{8\sqrt[4]{25^{3/4}}\pi e^{\phi_4}}{11\sqrt{3}}$.

model 13	$U(4) \times U(2)_L \times U(2)_R \times USp(2)$								
stack	N	$(n^1, l^1) \times (n^2, l^2) \times (n^3, l^3)$	$n_{\square\square}$	n_{\square}	b	b'	c	c'	1
a	8	$(1, 1) \times (1, 0) \times (1, -1)$	0	0	0	3	-6	3	0
b	4	$(1, 1) \times (1, 1) \times (1, -2)$	2	6	-	-	-8	0	2
c	4	$(1, 5) \times (0, 1) \times (-1, -2)$	-9	9	-	-	-	-	10
1	2	$(1, 0) \times (1, 0) \times (2, 0)$	$x_A = \frac{1}{12}x_B = \frac{1}{10}x_C = \frac{1}{12}x_D$ $\beta_1^g = 6$ $\chi_1 = \frac{1}{\sqrt{10}}, \chi_2 = \frac{\sqrt{\frac{5}{2}}}{6}, \chi_3 = \sqrt{\frac{2}{5}}$						

Table 24. D6-brane configurations and intersection numbers of Model 14, and its MSSM gauge coupling relation is $g_a^2 = \frac{7}{6}g_b^2 = \frac{35}{66}g_c^2 = \frac{175}{268}(\frac{5}{3}g_Y^2) = \frac{8\sqrt{25^{3/4}}\pi e^{\phi_4}}{11\sqrt{3}}$.

model 14	$U(4) \times U(2)_L \times U(2)_R \times USp(2)$								
stack	N	$(n^1, l^1) \times (n^2, l^2) \times (n^3, l^3)$	$n_{\square\square}$	n_{\square}	b	b'	c	c'	1
a	8	$(1, 1) \times (1, 0) \times (1, -1)$	0	0	0	3	-6	3	0
b	4	$(1, 1) \times (1, 1) \times (1, -2)$	2	6	-	-	-8	0	2
c	4	$(-1, -5) \times (0, 1) \times (1, 2)$	-9	9	-	-	-	0	10
1	2	$(1, 0) \times (1, 0) \times (2, 0)$	$x_A = \frac{1}{12}x_B = \frac{1}{10}x_C = \frac{1}{12}x_D$ $\beta_1^g = 6$ $\chi_1 = \frac{1}{\sqrt{10}}, \chi_2 = \frac{\sqrt{5}}{6}, \chi_3 = \sqrt{\frac{2}{5}}$						

Table 25. D6-brane configurations and intersection numbers of Model 15, and its MSSM gauge coupling relation is $g_a^2 = \frac{11}{6}g_b^2 = \frac{5}{14}g_c^2 = \frac{25}{52}(\frac{5}{3}g_Y^2) = \frac{8}{63}5^{3/4}\sqrt{11}\pi e^{\phi_4}$.

model 15	$U(4) \times U(2)_L \times U(2)_R \times USp(2)^2$										
stack	N	$(n^1, l^1) \times (n^2, l^2) \times (n^3, l^3)$	$n_{\square\square}$	n_{\square}	b	b'	c	c'	1	4	
a	8	$(-1, 1) \times (-1, 1) \times (-1, 1)$	0	4	3	0	3	-6	1	1	
b	4	$(2, 1) \times (0, 1) \times (-1, -1)$	1	-1	-	-	10	-9	1	0	
c	4	$(-1, 2) \times (-1, 0) \times (5, 1)$	9	-9	-	-	-	-	0	1	
1	2	$(1, 0) \times (1, 0) \times (2, 0)$	$x_A = 22x_B = 2x_C = \frac{11}{5}x_D$ $\beta_1^g = -3, \beta_4^g = -3$ $\chi_1 = \frac{1}{\sqrt{5}}, \chi_2 = \frac{11}{\sqrt{5}}, \chi_3 = 4\sqrt{5}$								
4	2	$(0, 1) \times (0, 1) \times (2, 0)$									

Table 26. D6-brane configurations and intersection numbers of Model 16, and its MSSM gauge coupling relation is $g_a^2 = \frac{11}{6}g_b^2 = \frac{5}{14}g_c^2 = \frac{25}{52}(\frac{5}{3}g_Y^2) = \frac{8}{63}5^{3/4}\sqrt{11}\pi e^{\phi_4}$.

model 16	$U(4) \times U(2)_L \times U(2)_R \times USp(2)^2$										
stack	N	$(n^1, l^1) \times (n^2, l^2) \times (n^3, l^3)$	$n_{\square\square}$	n_{\square}	b	b'	c	c'	1	4	
a	8	$(-1, 1) \times (-1, 1) \times (-1, 1)$	0	4	0	3	-6	3	1	1	
b	4	$(-2, 1) \times (0, 1) \times (-1, 1)$	-1	1	-	-	-10	9	1	0	
c	4	$(1, 2) \times (-1, 0) \times (-5, 1)$	-9	9	-	-	-	-	0	1	
1	2	$(1, 0) \times (1, 0) \times (2, 0)$	$x_A = 22x_B = 2x_C = \frac{11}{5}x_D$ $\beta_1^g = -3, \beta_4^g = -3$ $\chi_1 = \frac{1}{\sqrt{5}}, \chi_2 = \frac{11}{\sqrt{5}}, \chi_3 = 4\sqrt{5}$								
4	2	$(0, 1) \times (0, 1) \times (2, 0)$									

Table 27. D6-brane configurations and intersection numbers of Model 17, and its MSSM gauge coupling relation is $g_a^2 = \frac{11}{6}g_b^2 = \frac{5}{14}g_c^2 = \frac{25}{52}(\frac{5}{3}g_Y^2) = \frac{8}{63}5^{3/4}\sqrt{11}\pi e^{\phi_4}$.

model 17		$U(4) \times U(2)_L \times U(2)_R \times USp(2)^2$									
stack	N	$(n^1, l^1) \times (n^2, l^2) \times (n^3, l^3)$	$n_{\square\square}$	n_{\square}	b	b'	c	c'	1	4	
a	8	$(-1, 1) \times (-1, 1) \times (-1, 1)$	0	4	3	0	-6	3	1	1	
b	4	$(2, 1) \times (0, 1) \times (-1, -1)$	1	-1	-	-	-9	10	1	0	
c	4	$(1, 2) \times (-1, 0) \times (-5, 1)$	-9	9	-	-	-	-	0	1	
1	2	$(1, 0) \times (1, 0) \times (2, 0)$	$x_A = 22x_B = 2x_C = \frac{11}{5}x_D$ $\beta_1^g = -3, \beta_4^g = -3$ $\chi_1 = \frac{1}{\sqrt{5}}, \chi_2 = \frac{11}{\sqrt{5}}, \chi_3 = 4\sqrt{5}$								
4	2	$(0, 1) \times (0, 1) \times (2, 0)$									

Table 28. D6-brane configurations and intersection numbers of Model 18, and its MSSM gauge coupling relation is $g_a^2 = \frac{11}{6}g_b^2 = \frac{5}{14}g_c^2 = \frac{25}{52}(\frac{5}{3}g_Y^2) = \frac{8}{63}5^{3/4}\sqrt{11}\pi e^{\phi_4}$.

model 18		$U(4) \times U(2)_L \times U(2)_R \times USp(2)^2$									
stack	N	$(n^1, l^1) \times (n^2, l^2) \times (n^3, l^3)$	$n_{\square\square}$	n_{\square}	b	b'	c	c'	1	4	
a	8	$(-1, 1) \times (-1, 1) \times (-1, 1)$	0	4	0	3	3	-6	1	1	
b	4	$(-2, 1) \times (0, 1) \times (-1, 1)$	-1	1	-	-	9	-10	1	0	
c	4	$(1, -2) \times (1, 0) \times (5, 1)$	9	-9	-	-	-	-	0	1	
1	2	$(1, 0) \times (1, 0) \times (2, 0)$	$x_A = 22x_B = 2x_C = \frac{11}{5}x_D$ $\beta_1^g = -3, \beta_4^g = -3$ $\chi_1 = \frac{1}{\sqrt{5}}, \chi_2 = \frac{11}{\sqrt{5}}, \chi_3 = 4\sqrt{5}$								
4	2	$(0, 1) \times (0, 1) \times (2, 0)$									

Table 29. D6-brane configurations and intersection numbers of Model 19, and its MSSM gauge coupling relation is $g_a^2 = \frac{11}{6}g_b^2 = \frac{5}{14}g_c^2 = \frac{25}{52}(\frac{5}{3}g_Y^2) = \frac{8}{63}5^{3/4}\sqrt{11}\pi e^{\phi_4}$.

model 19		$U(4) \times U(2)_L \times U(2)_R \times USp(2)^2$									
stack	N	$(n^1, l^1) \times (n^2, l^2) \times (n^3, l^3)$	$n_{\square\square}$	n_{\square}	b	b'	c	c'	1	4	
a	8	$(-1, 1) \times (-1, 1) \times (-1, 1)$	0	4	3	0	3	-6	1	1	
b	4	$(2, 1) \times (0, 1) \times (-1, -1)$	1	-1	-	-	10	-9	1	0	
c	4	$(1, -2) \times (1, 0) \times (5, 1)$	9	-9	-	-	-	-	0	1	
1	2	$(1, 0) \times (1, 0) \times (2, 0)$	$x_A = 22x_B = 2x_C = \frac{11}{5}x_D$ $\beta_1^g = -3, \beta_4^g = -3$ $\chi_1 = \frac{1}{\sqrt{5}}, \chi_2 = \frac{11}{\sqrt{5}}, \chi_3 = 4\sqrt{5}$								
4	2	$(0, 1) \times (0, 1) \times (2, 0)$									

Table 30. D6-brane configurations and intersection numbers of Model 20, and its MSSM gauge coupling relation is $g_a^2 = \frac{11}{6}g_b^2 = \frac{5}{14}g_c^2 = \frac{25}{52}(\frac{5}{3}g_Y^2) = \frac{8}{63}5^{3/4}\sqrt{11}\pi e^{\phi_4}$.

model 20		$U(4) \times U(2)_L \times U(2)_R \times USp(2)^2$									
stack	N	$(n^1, l^1) \times (n^2, l^2) \times (n^3, l^3)$	$n_{\square\square}$	n_{\square}	b	b'	c	c'	1	4	
a	8	$(-1, 1) \times (-1, 1) \times (-1, 1)$	0	4	0	3	-6	3	1	1	
b	4	$(-2, 1) \times (0, 1) \times (-1, 1)$	-1	1	-	-	-10	9	1	0	
c	4	$(-1, -2) \times (1, 0) \times (-5, 1)$	-9	9	-	-	-	-	0	1	
1	2	$(1, 0) \times (1, 0) \times (2, 0)$	$x_A = 22x_B = 2x_C = \frac{11}{5}x_D$ $\beta_1^g = -3, \beta_4^g = -3$ $\chi_1 = \frac{1}{\sqrt{5}}, \chi_2 = \frac{11}{\sqrt{5}}, \chi_3 = 4\sqrt{5}$								
4	2	$(0, 1) \times (0, 1) \times (2, 0)$									

Table 31. D6-brane configurations and intersection numbers of Model 21, and its MSSM gauge coupling relation is $g_a^2 = \frac{11}{6}g_b^2 = \frac{5}{14}g_c^2 = \frac{25}{52}(\frac{5}{3}g_Y^2) = \frac{8}{63}5^{3/4}\sqrt{11}\pi e^{\phi_4}$.

model 21		$U(4) \times U(2)_L \times U(2)_R \times USp(2)^2$									
stack	N	$(n^1, l^1) \times (n^2, l^2) \times (n^3, l^3)$	$n_{\square\square}$	n_{\square}	b	b'	c	c'	1	4	
a	8	$(-1, 1) \times (-1, 1) \times (-1, 1)$	0	4	3	0	-6	3	1	1	
b	4	$(2, 1) \times (0, 1) \times (-1, -1)$	1	-1	-	-	-9	10	1	0	
c	4	$(-1, -2) \times (1, 0) \times (-5, 1)$	-9	9	-	-	-	-	0	1	
1	2	$(1, 0) \times (1, 0) \times (2, 0)$	$x_A = 22x_B = 2x_C = \frac{11}{5}x_D$ $\beta_1^g = -3, \beta_4^g = -3$ $\chi_1 = \frac{1}{\sqrt{5}}, \chi_2 = \frac{11}{\sqrt{5}}, \chi_3 = 4\sqrt{5}$								
4	2	$(0, 1) \times (0, 1) \times (2, 0)$									

Table 32. D6-brane configurations and intersection numbers of Model 22, and its MSSM gauge coupling relation is $g_a^2 = \frac{11}{6}g_b^2 = \frac{5}{14}g_c^2 = \frac{25}{52}(\frac{5}{3}g_Y^2) = \frac{8}{63}5^{3/4}\sqrt{11}\pi e^{\phi_4}$.

model 22		$U(4) \times U(2)_L \times U(2)_R \times USp(2)^2$									
stack	N	$(n^1, l^1) \times (n^2, l^2) \times (n^3, l^3)$	$n_{\square\square}$	n_{\square}	b	b'	c	c'	1	4	
a	8	$(-1, 1) \times (-1, 1) \times (-1, 1)$	0	4	0	3	-6	3	1	1	
b	4	$(-2, 1) \times (0, 1) \times (-1, 1)$	-1	1	-	-	-10	9	1	0	
c	4	$(1, 2) \times (1, 0) \times (5, -1)$	-9	9	-	-	-	-	0	1	
1	2	$(1, 0) \times (1, 0) \times (2, 0)$	$x_A = 22x_B = 2x_C = \frac{11}{5}x_D$ $\beta_1^g = -3, \beta_4^g = -3$ $\chi_1 = \frac{1}{\sqrt{5}}, \chi_2 = \frac{11}{\sqrt{5}}, \chi_3 = 4\sqrt{5}$								
4	2	$(0, 1) \times (0, 1) \times (2, 0)$									

Table 33. D6-brane configurations and intersection numbers of Model 23, and its MSSM gauge coupling relation is $g_a^2 = \frac{11}{6}g_b^2 = \frac{5}{14}g_c^2 = \frac{25}{52}(\frac{5}{3}g_Y^2) = \frac{8}{63}5^{3/4}\sqrt{11}\pi e^{\phi_4}$.

model 23		$U(4) \times U(2)_L \times U(2)_R \times USp(2)^2$									
stack	N	$(n^1, l^1) \times (n^2, l^2) \times (n^3, l^3)$	$n_{\square\square}$	n_{\square}	b	b'	c	c'	1	4	
a	8	$(-1, 1) \times (-1, 1) \times (-1, 1)$	0	4	3	0	-6	3	1	1	
b	4	$(2, 1) \times (0, 1) \times (-1, -1)$	1	-1	-	-	-9	10	1	0	
c	4	$(1, 2) \times (1, 0) \times (5, -1)$	-9	9	-	-	-	-	0	1	
1	2	$(1, 0) \times (1, 0) \times (2, 0)$	$x_A = 22x_B = 2x_C = \frac{11}{5}x_D$ $\beta_1^g = -3, \beta_4^g = -3$ $\chi_1 = \frac{1}{\sqrt{5}}, \chi_2 = \frac{11}{\sqrt{5}}, \chi_3 = 4\sqrt{5}$								
4	2	$(0, 1) \times (0, 1) \times (2, 0)$									

Table 34. D6-brane configurations and intersection numbers of Model 24, and its MSSM gauge coupling relation is $g_a^2 = \frac{11}{6}g_b^2 = \frac{5}{14}g_c^2 = \frac{25}{52}(\frac{5}{3}g_Y^2) = \frac{8}{63}5^{3/4}\sqrt{11}\pi e^{\phi_4}$.

model 24		$U(4) \times U(2)_L \times U(2)_R \times USp(2)^2$									
stack	N	$(n^1, l^1) \times (n^2, l^2) \times (n^3, l^3)$	$n_{\square\square}$	n_{\square}	b	b'	c	c'	1	4	
a	8	$(-1, 1) \times (-1, 1) \times (-1, 1)$	0	4	0	3	3	-6	1	1	
b	4	$(-2, 1) \times (0, 1) \times (-1, 1)$	-1	1	-	-	9	-10	1	0	
c	4	$(-1, 2) \times (1, 0) \times (-5, -1)$	9	-9	-	-	-	-	0	1	
1	2	$(1, 0) \times (1, 0) \times (2, 0)$	$x_A = 22x_B = 2x_C = \frac{11}{5}x_D$ $\beta_1^g = -3, \beta_4^g = -3$ $\chi_1 = \frac{1}{\sqrt{5}}, \chi_2 = \frac{11}{\sqrt{5}}, \chi_3 = 4\sqrt{5}$								
4	2	$(0, 1) \times (0, 1) \times (2, 0)$									

Table 35. D6-brane configurations and intersection numbers of Model 25, and its MSSM gauge coupling relation is $g_a^2 = 3g_b^2 = \frac{13}{5}g_c^2 = \frac{65}{41}(\frac{5}{3}g_Y^2) = \frac{16}{5}\sqrt{3}\pi e^{\phi_4}$.

model 25		$U(4) \times U(2)_L \times U(2)_R \times USp(2) \times USp(4)$									
stack	N	$(n^1, l^1) \times (n^2, l^2) \times (n^3, l^3)$	$n_{\square\square}$	n_{\square}	b	b'	c	c'	1	3	
a	8	$(-1, 1) \times (-1, 0) \times (1, 1)$	0	0	0	3	-1	-2	0	0	
b	4	$(1, 4) \times (0, 1) \times (-1, -1)$	-3	3	-	-	-4	8	4	1	
c	4	$(1, 0) \times (1, -1) \times (1, 3)$	-2	2	-	-	-	-	0	1	
1	2	$(1, 0) \times (1, 0) \times (2, 0)$	$x_A = \frac{3}{4}x_B = \frac{1}{4}x_C = \frac{3}{4}x_D$ $\beta_1^g = -2, \beta_3^g = -4$ $\chi_1 = \frac{1}{2}, \chi_2 = \frac{3}{2}, \chi_3 = 1$								
3	4	$(0, 1) \times (1, 0) \times (0, 2)$									

Table 36. D6-brane configurations and intersection numbers of Model 26, and its MSSM gauge coupling relation is $g_a^2 = 3g_b^2 = \frac{13}{5}g_c^2 = \frac{65}{41}(\frac{5}{3}g_Y^2) = \frac{16}{5}\sqrt{3}\pi e^{\phi_4}$.

model 26		$U(4) \times U(2)_L \times U(2)_R \times USp(2) \times USp(4)$									
stack	N	$(n^1, l^1) \times (n^2, l^2) \times (n^3, l^3)$	$n_{\square\square}$	n_{\square}	b	b'	c	c'	1	3	
a	8	$(-1, 1) \times (-1, 0) \times (1, 1)$	0	0	3	0	-2	-1	0	0	
b	4	$(-1, 4) \times (0, 1) \times (-1, 1)$	3	-3	-	-	4	-8	4	1	
c	4	$(1, 0) \times (1, 1) \times (1, -3)$	2	-2	-	-	-	-	0	1	
1	2	$(1, 0) \times (1, 0) \times (2, 0)$	$x_A = \frac{3}{4}x_B = \frac{1}{4}x_C = \frac{3}{4}x_D$ $\beta_1^g = -2, \beta_3^g = -4$ $\chi_1 = \frac{1}{2}, \chi_2 = \frac{3}{2}, \chi_3 = 1$								
3	4	$(0, 1) \times (1, 0) \times (0, 2)$									

Table 37. D6-brane configurations and intersection numbers of Model 27, and its MSSM gauge coupling relation is $g_a^2 = 3g_b^2 = \frac{13}{5}g_c^2 = \frac{65}{41}(\frac{5}{3}g_Y^2) = \frac{16}{5}\sqrt{3}\pi e^{\phi_4}$.

model 27		$U(4) \times U(2)_L \times U(2)_R \times USp(2) \times USp(4)$									
stack	N	$(n^1, l^1) \times (n^2, l^2) \times (n^3, l^3)$	$n_{\square\square}$	n_{\square}	b	b'	c	c'	1	3	
a	8	$(-1, 1) \times (-1, 0) \times (1, 1)$	0	0	0	3	-2	-1	0	0	
b	4	$(1, 4) \times (0, 1) \times (-1, -1)$	-3	3	-	-	8	-4	4	1	
c	4	$(1, 0) \times (1, 1) \times (1, -3)$	2	-2	-	-	-	-	0	1	
1	2	$(1, 0) \times (1, 0) \times (2, 0)$	$x_A = \frac{3}{4}x_B = \frac{1}{4}x_C = \frac{3}{4}x_D$ $\beta_1^g = -2, \beta_3^g = -4$ $\chi_1 = \frac{1}{2}, \chi_2 = \frac{3}{2}, \chi_3 = 1$								
3	4	$(0, 1) \times (1, 0) \times (0, 2)$									

Table 38. D6-brane configurations and intersection numbers of Model 28, and its MSSM gauge coupling relation is $g_a^2 = 3g_b^2 = \frac{13}{5}g_c^2 = \frac{65}{41}(\frac{5}{3}g_Y^2) = \frac{16}{5}\sqrt{3}\pi e^{\phi_4}$.

model 28		$U(4) \times U(2)_L \times U(2)_R \times USp(2) \times USp(4)$									
stack	N	$(n^1, l^1) \times (n^2, l^2) \times (n^3, l^3)$	$n_{\square\square}$	n_{\square}	b	b'	c	c'	1	3	
a	8	$(-1, 1) \times (-1, 0) \times (1, 1)$	0	0	3	0	-1	-2	0	0	
b	4	$(-1, 4) \times (0, 1) \times (-1, 1)$	3	-3	-	-	-8	4	4	1	
c	4	$(-1, 0) \times (-1, 1) \times (1, 3)$	-2	2	-	-	-	-	0	1	
1	2	$(1, 0) \times (1, 0) \times (2, 0)$	$x_A = \frac{3}{4}x_B = \frac{1}{4}x_C = \frac{3}{4}x_D$ $\beta_1^g = -2, \beta_3^g = -4$ $\chi_1 = \frac{1}{2}, \chi_2 = \frac{3}{2}, \chi_3 = 1$								
3	4	$(0, 1) \times (1, 0) \times (0, 2)$									

Table 39. D6-brane configurations and intersection numbers of Model 29, and its MSSM gauge coupling relation is $g_a^2 = 3g_b^2 = \frac{13}{5}g_c^2 = \frac{65}{41}(\frac{5}{3}g_Y^2) = \frac{16}{5}\sqrt{3}\pi e^{\phi_4}$.

model 29		$U(4) \times U(2)_L \times U(2)_R \times USp(2) \times USp(4)$									
stack	N	$(n^1, l^1) \times (n^2, l^2) \times (n^3, l^3)$	$n_{\square\square}$	n_{\square}	b	b'	c	c'	1	3	
a	8	$(-1, 1) \times (-1, 0) \times (1, 1)$	0	0	0	3	-1	-2	0	0	
b	4	$(1, 4) \times (0, 1) \times (-1, -1)$	-3	3	-	-	-4	8	4	1	
c	4	$(-1, 0) \times (-1, 1) \times (1, 3)$	-2	2	-	-	-	-	0	1	
1	2	$(1, 0) \times (1, 0) \times (2, 0)$	$x_A = \frac{3}{4}x_B = \frac{1}{4}x_C = \frac{3}{4}x_D$ $\beta_1^g = -2, \beta_3^g = -4$ $\chi_1 = \frac{1}{2}, \chi_2 = \frac{3}{2}, \chi_3 = 1$								
3	4	$(0, 1) \times (1, 0) \times (0, 2)$									

Table 40. D6-brane configurations and intersection numbers of Model 30, and its MSSM gauge coupling relation is $g_a^2 = 3g_b^2 = \frac{13}{5}g_c^2 = \frac{65}{41}(\frac{5}{3}g_Y^2) = \frac{16}{5}\sqrt{3}\pi e^{\phi_4}$.

model 30		$U(4) \times U(2)_L \times U(2)_R \times USp(2) \times USp(4)$									
stack	N	$(n^1, l^1) \times (n^2, l^2) \times (n^3, l^3)$	$n_{\square\square}$	n_{\square}	b	b'	c	c'	1	3	
a	8	$(-1, 1) \times (-1, 0) \times (1, 1)$	0	0	3	0	-2	-1	0	0	
b	4	$(-1, 4) \times (0, 1) \times (-1, 1)$	3	-3	-	-	4	-8	4	1	
c	4	$(-1, 0) \times (-1, -1) \times (1, -3)$	2	-2	-	-	-	-	0	1	
1	2	$(1, 0) \times (1, 0) \times (2, 0)$	$x_A = \frac{3}{4}x_B = \frac{1}{4}x_C = \frac{3}{4}x_D$ $\beta_1^g = -2, \beta_3^g = -4$ $\chi_1 = \frac{1}{2}, \chi_2 = \frac{3}{2}, \chi_3 = 1$								
3	4	$(0, 1) \times (1, 0) \times (0, 2)$									

Table 41. D6-brane configurations and intersection numbers of Model 31, and its MSSM gauge coupling relation is $g_a^2 = 3g_b^2 = \frac{13}{5}g_c^2 = \frac{65}{41}(\frac{5}{3}g_Y^2) = \frac{16}{5}\sqrt{3}\pi e^{\phi_4}$.

model 31		$U(4) \times U(2)_L \times U(2)_R \times USp(2) \times USp(4)$									
stack	N	$(n^1, l^1) \times (n^2, l^2) \times (n^3, l^3)$	$n_{\square\square}$	n_{\square}	b	b'	c	c'	1	3	
a	8	$(-1, 1) \times (-1, 0) \times (1, 1)$	0	0	0	3	-2	-1	0	0	
b	4	$(1, 4) \times (0, 1) \times (-1, -1)$	-3	3	-	-	8	-4	4	1	
c	4	$(-1, 0) \times (-1, -1) \times (1, -3)$	2	-2	-	-	-	-	0	1	
1	2	$(1, 0) \times (1, 0) \times (2, 0)$	$x_A = \frac{3}{4}x_B = \frac{1}{4}x_C = \frac{3}{4}x_D$ $\beta_1^g = -2, \beta_3^g = -4$ $\chi_1 = \frac{1}{2}, \chi_2 = \frac{3}{2}, \chi_3 = 1$								
3	4	$(0, 1) \times (1, 0) \times (0, 2)$									

Table 42. D6-brane configurations and intersection numbers of Model 32, and its MSSM gauge coupling relation is $g_a^2 = 3g_b^2 = \frac{13}{5}g_c^2 = \frac{65}{41}(\frac{5}{3}g_Y^2) = \frac{16}{5}\sqrt{3}\pi e^{\phi_4}$.

model 32		$U(4) \times U(2)_L \times U(2)_R \times USp(2) \times USp(4)$									
stack	N	$(n^1, l^1) \times (n^2, l^2) \times (n^3, l^3)$	$n_{\square\square}$	n_{\square}	b	b'	c	c'	1	3	
a	8	$(-1, 1) \times (-1, 0) \times (1, 1)$	0	0	3	0	-2	-1	0	0	
b	4	$(-1, 4) \times (0, 1) \times (-1, 1)$	3	-3	-	-	4	-8	4	1	
c	4	$(-1, 0) \times (1, 1) \times (-1, 3)$	2	-2	-	-	-	-	0	1	
1	2	$(1, 0) \times (1, 0) \times (2, 0)$	$x_A = \frac{3}{4}x_B = \frac{1}{4}x_C = \frac{3}{4}x_D$ $\beta_1^g = -2, \beta_3^g = -4$ $\chi_1 = \frac{1}{2}, \chi_2 = \frac{3}{2}, \chi_3 = 1$								
3	4	$(0, 1) \times (1, 0) \times (0, 2)$									

Table 43. D6-brane configurations and intersection numbers of Model 33, and its MSSM gauge coupling relation is $g_a^2 = 3g_b^2 = \frac{13}{5}g_c^2 = \frac{65}{41}(\frac{5}{3}g_Y^2) = \frac{16}{5}\sqrt{3}\pi e^{\phi_4}$.

model 33	$U(4) \times U(2)_L \times U(2)_R \times USp(2) \times USp(4)$									
stack	N	$(n^1, l^1) \times (n^2, l^2) \times (n^3, l^3)$	$n_{\square\square}$	n_{\square}	b	b'	c	c'	1	3
a	8	$(-1, 1) \times (-1, 0) \times (1, 1)$	0	0	0	3	-2	-1	0	0
b	4	$(1, 4) \times (0, 1) \times (-1, -1)$	-3	3	-	-	8	-4	4	1
c	4	$(-1, 0) \times (1, 1) \times (-1, 3)$	2	-2	-	-	-	-	0	1
1	2	$(1, 0) \times (1, 0) \times (2, 0)$	$x_A = \frac{3}{4}x_B = \frac{1}{4}x_C = \frac{3}{4}x_D$ $\beta_1^g = -2, \beta_3^g = -4$ $\chi_1 = \frac{1}{2}, \chi_2 = \frac{3}{2}, \chi_3 = 1$							
3	4	$(0, 1) \times (1, 0) \times (0, 2)$								

Table 44. D6-brane configurations and intersection numbers of Model 34, and its MSSM gauge coupling relation is $g_a^2 = 3g_b^2 = \frac{13}{5}g_c^2 = \frac{65}{41}(\frac{5}{3}g_Y^2) = \frac{16}{5}\sqrt{3}\pi e^{\phi_4}$.

model 34	$U(4) \times U(2)_L \times U(2)_R \times USp(2) \times USp(4)$									
stack	N	$(n^1, l^1) \times (n^2, l^2) \times (n^3, l^3)$	$n_{\square\square}$	n_{\square}	b	b'	c	c'	1	3
a	8	$(-1, 1) \times (-1, 0) \times (1, 1)$	0	0	3	0	-1	-2	0	0
b	4	$(-1, 4) \times (0, 1) \times (-1, 1)$	3	-3	-	-	-8	4	4	1
c	4	$(-1, 0) \times (1, -1) \times (-1, -3)$	-2	2	-	-	-	-	0	1
1	2	$(1, 0) \times (1, 0) \times (2, 0)$	$x_A = \frac{3}{4}x_B = \frac{1}{4}x_C = \frac{3}{4}x_D$ $\beta_1^g = -2, \beta_3^g = -4$ $\chi_1 = \frac{1}{2}, \chi_2 = \frac{3}{2}, \chi_3 = 1$							
3	4	$(0, 1) \times (1, 0) \times (0, 2)$								

Table 45. D6-brane configurations and intersection numbers of Model 35, and its MSSM gauge coupling relation is $g_a^2 = 6g_b^2 = \frac{26}{5}g_c^2 = \frac{130}{67}(\frac{5}{3}g_Y^2) = \frac{16}{5}\sqrt{6}\pi e^{\phi_4}$.

model 35	$U(4) \times U(2)_L \times U(2)_R \times USp(4)$									
stack	N	$(n^1, l^1) \times (n^2, l^2) \times (n^3, l^3)$	$n_{\square\square}$	n_{\square}	b	b'	c	c'	3	
a	8	$(-1, 1) \times (-1, 0) \times (1, 1)$	0	0	0	3	-1	-2	0	
b	4	$(1, 4) \times (0, 1) \times (-1, -1)$	-3	3	-	-	-8	16	1	
c	4	$(1, 0) \times (2, -1) \times (1, 3)$	-5	5	-	-	-	-	1	
3	4	$(0, 1) \times (1, 0) \times (0, 2)$	$x_A = \frac{3}{2}x_B = \frac{1}{4}x_C = \frac{3}{2}x_D$ $\beta_3^g = -4$ $\chi_1 = \frac{1}{2}, \chi_2 = 3, \chi_3 = 1$							

Table 46. D6-brane configurations and intersection numbers of Model 36, and its MSSM gauge coupling relation is $g_a^2 = 6g_b^2 = \frac{26}{5}g_c^2 = \frac{130}{67}(\frac{5}{3}g_Y^2) = \frac{16}{5}\sqrt{6}\pi e^{\phi_4}$.

model 36	$U(4) \times U(2)_L \times U(2)_R \times USp(4)$									
stack	N	$(n^1, l^1) \times (n^2, l^2) \times (n^3, l^3)$	$n_{\square\square}$	n_{\square}	b	b'	c	c'	3	
a	8	$(-1, 1) \times (-1, 0) \times (1, 1)$	0	0	3	0	-2	-1	0	
b	4	$(-1, 4) \times (0, 1) \times (-1, 1)$	3	-3	-	-	8	-16	1	
c	4	$(1, 0) \times (2, 1) \times (1, -3)$	5	-5	-	-	-	-	1	
3	4	$(0, 1) \times (1, 0) \times (0, 2)$	$x_A = \frac{3}{2}x_B = \frac{1}{4}x_C = \frac{3}{2}x_D$ $\beta_3^g = -4$ $\chi_1 = \frac{1}{2}, \chi_2 = 3, \chi_3 = 1$							

Table 47. D6-brane configurations and intersection numbers of Model 37, and its MSSM gauge coupling relation is $g_a^2 = 6g_b^2 = \frac{26}{5}g_c^2 = \frac{130}{67}(\frac{5}{3}g_Y^2) = \frac{16}{5}\sqrt{6}\pi e^{\phi_4}$.

model 37	$U(4) \times U(2)_L \times U(2)_R \times USp(4)$								
stack	N	$(n^1, l^1) \times (n^2, l^2) \times (n^3, l^3)$	$n_{\square\square}$	n_{\square}	b	b'	c	c'	3
a	8	$(-1, 1) \times (-1, 0) \times (1, 1)$	0	0	0	3	-2	-1	0
b	4	$(1, 4) \times (0, 1) \times (-1, -1)$	-3	3	-	-	16	-8	1
c	4	$(1, 0) \times (2, 1) \times (1, -3)$	5	-5	-	-	-	-	1
3	4	$(0, 1) \times (1, 0) \times (0, 2)$	$x_A = \frac{3}{2}x_B = \frac{1}{4}x_C = \frac{3}{2}x_D$ $\beta_3^g = -4$ $\chi_1 = \frac{1}{2}, \chi_2 = 3, \chi_3 = 1$						

Table 48. D6-brane configurations and intersection numbers of Model 38, and its MSSM gauge coupling relation is $g_a^2 = 6g_b^2 = \frac{26}{5}g_c^2 = \frac{130}{67}(\frac{5}{3}g_Y^2) = \frac{16}{5}\sqrt{6}\pi e^{\phi_4}$.

model 38	$U(4) \times U(2)_L \times U(2)_R \times USp(4)$								
stack	N	$(n^1, l^1) \times (n^2, l^2) \times (n^3, l^3)$	$n_{\square\square}$	n_{\square}	b	b'	c	c'	3
a	8	$(-1, 1) \times (-1, 0) \times (1, 1)$	0	0	3	0	-1	-2	0
b	4	$(-1, 4) \times (0, 1) \times (-1, 1)$	3	-3	-	-	-16	8	1
c	4	$(-1, 0) \times (-2, 1) \times (1, 3)$	-5	5	-	-	-	-	1
3	4	$(0, 1) \times (1, 0) \times (0, 2)$	$x_A = \frac{3}{2}x_B = \frac{1}{4}x_C = \frac{3}{2}x_D$ $\beta_3^g = -4$ $\chi_1 = \frac{1}{2}, \chi_2 = 3, \chi_3 = 1$						

Table 49. D6-brane configurations and intersection numbers of Model 39, and its MSSM gauge coupling relation is $g_a^2 = 6g_b^2 = \frac{26}{5}g_c^2 = \frac{130}{67}(\frac{5}{3}g_Y^2) = \frac{16}{5}\sqrt{6}\pi e^{\phi_4}$.

model 39	$U(4) \times U(2)_L \times U(2)_R \times USp(4)$								
stack	N	$(n^1, l^1) \times (n^2, l^2) \times (n^3, l^3)$	$n_{\square\square}$	n_{\square}	b	b'	c	c'	3
a	8	$(-1, 1) \times (-1, 0) \times (1, 1)$	0	0	0	3	-1	-2	0
b	4	$(1, 4) \times (0, 1) \times (-1, -1)$	-3	3	-	-	-8	16	1
c	4	$(-1, 0) \times (-2, 1) \times (1, 3)$	-5	5	-	-	-	-	1
3	4	$(0, 1) \times (1, 0) \times (0, 2)$	$x_A = \frac{3}{2}x_B = \frac{1}{4}x_C = \frac{3}{2}x_D$ $\beta_3^g = -4$ $\chi_1 = \frac{1}{2}, \chi_2 = 3, \chi_3 = 1$						

Table 50. D6-brane configurations and intersection numbers of Model 40, and its MSSM gauge coupling relation is $g_a^2 = 6g_b^2 = \frac{26}{5}g_c^2 = \frac{130}{67}(\frac{5}{3}g_Y^2) = \frac{16}{5}\sqrt{6}\pi e^{\phi_4}$.

model 40	$U(4) \times U(2)_L \times U(2)_R \times USp(4)$								
stack	N	$(n^1, l^1) \times (n^2, l^2) \times (n^3, l^3)$	$n_{\square\square}$	n_{\square}	b	b'	c	c'	3
a	8	$(-1, 1) \times (-1, 0) \times (1, 1)$	0	0	3	0	-2	-1	0
b	4	$(-1, 4) \times (0, 1) \times (-1, 1)$	3	-3	-	-	8	-16	1
c	4	$(-1, 0) \times (-2, -1) \times (1, -3)$	5	-5	-	-	-	-	1
3	4	$(0, 1) \times (1, 0) \times (0, 2)$	$x_A = \frac{3}{2}x_B = \frac{1}{4}x_C = \frac{3}{2}x_D$ $\beta_3^g = -4$ $\chi_1 = \frac{1}{2}, \chi_2 = 3, \chi_3 = 1$						

Table 51. D6-brane configurations and intersection numbers of Model 41, and its MSSM gauge coupling relation is $g_a^2 = 6g_b^2 = \frac{26}{5}g_c^2 = \frac{130}{67}(\frac{5}{3}g_Y^2) = \frac{16}{5}\sqrt{6}\pi e^{\phi_4}$.

model 41	$U(4) \times U(2)_L \times U(2)_R \times USp(4)$								
stack	N	$(n^1, l^1) \times (n^2, l^2) \times (n^3, l^3)$	$n_{\square\square}$	n_{\square}	b	b'	c	c'	3
a	8	$(-1, 1) \times (-1, 0) \times (1, 1)$	0	0	0	3	-2	-1	0
b	4	$(1, 4) \times (0, 1) \times (-1, -1)$	-3	3	-	-	16	-8	1
c	4	$(-1, 0) \times (-2, -1) \times (1, -3)$	5	-5	-	-	-	-	1
3	4	$(0, 1) \times (1, 0) \times (0, 2)$	$x_A = \frac{3}{2}x_B = \frac{1}{4}x_C = \frac{3}{2}x_D$ $\beta_3^g = -4$ $\chi_1 = \frac{1}{2}, \chi_2 = 3, \chi_3 = 1$						

Table 52. D6-brane configurations and intersection numbers of Model 42, and its MSSM gauge coupling relation is $g_a^2 = 6g_b^2 = \frac{26}{5}g_c^2 = \frac{130}{67}(\frac{5}{3}g_Y^2) = \frac{16}{5}\sqrt{6}\pi e^{\phi_4}$.

model 42	$U(4) \times U(2)_L \times U(2)_R \times USp(4)$								
stack	N	$(n^1, l^1) \times (n^2, l^2) \times (n^3, l^3)$	$n_{\square\square}$	n_{\square}	b	b'	c	c'	3
a	8	$(-1, 1) \times (-1, 0) \times (1, 1)$	0	0	3	0	-2	-1	0
b	4	$(-1, 4) \times (0, 1) \times (-1, 1)$	3	-3	-	-	8	-16	1
c	4	$(-1, 0) \times (2, 1) \times (-1, 3)$	5	-5	-	-	-	-	1
3	4	$(0, 1) \times (1, 0) \times (0, 2)$	$x_A = \frac{3}{2}x_B = \frac{1}{4}x_C = \frac{3}{2}x_D$ $\beta_3^g = -4$ $\chi_1 = \frac{1}{2}, \chi_2 = 3, \chi_3 = 1$						

Table 53. D6-brane configurations and intersection numbers of Model 43, and its MSSM gauge coupling relation is $g_a^2 = 6g_b^2 = \frac{26}{5}g_c^2 = \frac{130}{67}(\frac{5}{3}g_Y^2) = \frac{16}{5}\sqrt{6}\pi e^{\phi_4}$.

model 43	$U(4) \times U(2)_L \times U(2)_R \times USp(4)$								
stack	N	$(n^1, l^1) \times (n^2, l^2) \times (n^3, l^3)$	$n_{\square\square}$	n_{\square}	b	b'	c	c'	3
a	8	$(-1, 1) \times (-1, 0) \times (1, 1)$	0	0	0	3	-2	-1	0
b	4	$(1, 4) \times (0, 1) \times (-1, -1)$	-3	3	-	-	16	-8	1
c	4	$(-1, 0) \times (2, 1) \times (-1, 3)$	5	-5	-	-	-	-	1
3	4	$(0, 1) \times (1, 0) \times (0, 2)$	$x_A = \frac{3}{2}x_B = \frac{1}{4}x_C = \frac{3}{2}x_D$ $\beta_3^g = -4$ $\chi_1 = \frac{1}{2}, \chi_2 = 3, \chi_3 = 1$						

Table 54. D6-brane configurations and intersection numbers of Model 44, and its MSSM gauge coupling relation is $g_a^2 = 6g_b^2 = \frac{26}{5}g_c^2 = \frac{130}{67}(\frac{5}{3}g_Y^2) = \frac{16}{5}\sqrt{6}\pi e^{\phi_4}$.

model 44	$U(4) \times U(2)_L \times U(2)_R \times USp(4)$								
stack	N	$(n^1, l^1) \times (n^2, l^2) \times (n^3, l^3)$	$n_{\square\square}$	n_{\square}	b	b'	c	c'	3
a	8	$(-1, 1) \times (-1, 0) \times (1, 1)$	0	0	3	0	-1	-2	0
b	4	$(-1, 4) \times (0, 1) \times (-1, 1)$	3	-3	-	-	-16	8	1
c	4	$(-1, 0) \times (2, -1) \times (-1, -3)$	-5	5	-	-	-	-	1
3	4	$(0, 1) \times (1, 0) \times (0, 2)$	$x_A = \frac{3}{2}x_B = \frac{1}{4}x_C = \frac{3}{2}x_D$ $\beta_3^g = -4$ $\chi_1 = \frac{1}{2}, \chi_2 = 3, \chi_3 = 1$						